American Mineralogist, Volume 73, pages 775–797, 1988

Hydrothermal phlogopite and anhydrite from the SH2 well, Sabatini volcanic district, Latium, Italy: Fluid inclusions and mineral chemistry

Harvey E. Belkin
U.S. Geological Survey, 959 National Center, Reston, Virginia 22092, U.S.A.

Giuseppe Cavarretta
Centro di Studio per la Geologia dell'Italia Centrale del C.N.R., % Dipartimento di Scienze della Terra, Università degli Studi di Roma "La Sapienza," 00185, Roma, Italy

Benedetto De Vivo
Dipartimento di Geofisica e Vulcanologia, Largo S. Marcellino 10, 80138 Napoli, Italy

Francesca Tecce
Centro di Studio per la Geologia dell'Italia Centrale del C.N.R., % Dipartimento di Scienze della Terra, Università degli Studi di Roma "La Sapienza," 00185, Roma, Italy

Abstract

The SH2 well (2498.7 m) was drilled vertically in 1982–1983 by an AGIP-ENEL Joint Venture as an exploratory hole to assess the geothermal potential of the area north of Bracciano Lake, Latium, Italy, located in the Sabatini volcanic district. Drill-cutting samples from a thermometamorphic-metasomatic zone (1140–2498.7 m) contain hydrothermal anhydrite ± phlogopite (+ calcite ± pyrite) and other authigenic volatile-rich phases.

Microthermometry of primary and secondary two-phase [vapor (V) + liquid (L)] and multiphase (V + L + crystals) liquid-rich inclusions in anhydrite yields pressure-corrected temperatures of homogenization (trapping temperatures) that range from 144 to 304 °C and that are generally coincident with measured in-hole temperatures. The fluids have a variable salinity from 0.5 to 14.0 wt% NaCl equivalent and also contain Ca^{2+} at least. Rare liquid CO_2-bearing aqueous inclusions have been verified by laser Raman spectroscopy. Also, rare liquid hydrocarbons(?) have been observed. Clathrates have been observed upon freezing, and crushing studies reveal noncondensable gas at $P > 1$ atm in some inclusions. Euhedral to subhedral phlogopite crystals (~0.5 to ~2 mm) commonly are zoned and contain solid inclusions of anhydrite and apatite and two-phase (V + L) and multiphase (V + L + crystals) fluid inclusions. Microthermometry of primary two-phase inclusions yields pressure-corrected temperatures of homogenization (trapping temperatures) that range from 178 to 298 °C and are also generally coincident with in-hole measured temperatures. Freezing studies show a variable fluid salinity (0.2–7.8 wt% NaCl equiv.); the fluid contains Ca^{2+} at least. If we assume that the current hydrologic regime existed during anhydrite and phlogopite formation, the pressure of formation ranged from ~148 to ~220 bars for phlogopite (1600–~2500 m) and ~120 to ~220 bars for anhydrite (1300–~2500 m). Hence, the phlogopite and other authigenic phases have crystallized from a low *P–T,* volatile-rich, generally dilute, geothermal solution.

Detailed microprobe analyses of fluid inclusion–bearing phlogopites indicate that they are nearly end member, $Fe_T/(Fe_T + Mg) = 0.02$ to 0.1 and the $^{[4]}Al$ per 11 oxygen equivalents varies from 1.0 to 1.35. F, BaO, and TiO_2 range from 2.4 to 5.0 wt%, 0 to 3.5 wt%, and 0.1 to 0.89 wt%, respectively, and an Fe^{2+}-F avoidance is observed. Various cation substitutional schemes appear to be operative and are assessed. The dark zones are Fe-rich, but may have more or less F, BaO, or TiO_2 than the light zones. XRF-KEVEX analysis of eight anhydrite samples yield average values (ppm) of Sr = 5500, Ba = 1900, Rb = 250, Ce = 140, and La = 100.

The variation of fluid-inclusion salinities, the phlogopite zoning, and the chemical variation of the anhydrite and phlogopite suggest that different fluids and/or episodic conditions were operative in this geothermal system.

0003–004X/88/0708–0775$02.00

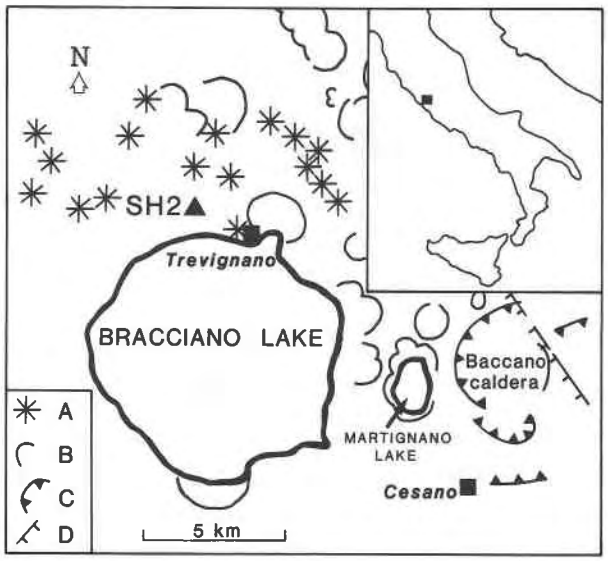

Fig. 1. Location of the SH2 well and the general features of the Sabatini volcanic district. A = scoria cones; B = explosive craters; C = caldera rims; D = fault.

Introduction

The Sabatini volcanic district, located in northern Latium, Italy, (Fig. 1) has recently received considerable attention by the AGIP-ENEL Joint Venture (National Oil and Electricity Boards, respectively; ENEL as operator) for geothermal energy exploration. The initial target area was the Cesano-Baccano caldera that has the highest geothermal gradient (100–150 °C/km; Calamai et al., 1975) of the region. From 1975 to date, 14 deep wells have been drilled. Four of them produced a hot supersaturated chloride-sulfate brine (200 °C, reservoir conditions) characterized by unusually high values of total dissolved salts (up to 400 g/L, postflash; flashing steam estimated to be 20–25% of total flow; Calamai et al., 1975). The difficulties inherent with the use of hot brines for electricity production have prompted the search for lower-salinity geothermal fluids outside the Cesano-Baccano caldera.

The SH2 deep well (2498.7 m) was drilled vertically in 1982–1983 as an exploratory hole to assess the geothermal potential of the area north of Bracciano Lake (Fig. 1). The bottom temperature was 290 °C, but no exploitable fluids were found (Calamai et al., 1985). Nevertheless, the pervasive hydrothermal alteration described by Cavarretta and Tecce (1987) is convincing evidence that an extensive hydrothermal system must have existed in the recent past. Extensive vein and pore-space fillings by hydrothermal minerals have effectively sealed the system. The lower 1630 m of the SH2 well is characterized by the hydrothermal assemblage anhydrite + calcite + pyrite plus, at various levels, the addition of K-feldspar, garnet, vesuvianite, apatite, phlogopite, spinel, pyroxene, wollastonite, and the occurrence of uncommon, volatile-rich minerals such as wilkeite, cuspidine, harkerite, cancrinite, and reyerite (Cavarretta and Tecce, 1987). On the basis of the various minerals recorded throughout the SH2 well, Cavarretta and Tecce (1987) have suggested that the ascending hydrothermal solutions were rich in SO_2 + CO_2 plus other volatiles (B, HF) and that perhaps a shallow Ca-rich fluid was present. They also have debated the hypothesis that the brine was, in part, the result of remobilization of sedimentary (Triassic) sulfates in a low-pressure environment. They have concluded that the hydrothermal solution and heat source was a magma of possible trachytic (or less differentiated) composition with a high volatile content that intruded in a subvolcanic environment in the northern Bracciano Lake area.

The study of fluid inclusions in hydrothermal minerals may allow an evaluation of the fluid composition, temperature, and hydrology at the time of trapping, thus providing information on the evolution of the geothermal systems (e.g., Browne et al., 1976; Taguchi and Hoyashi, 1983; Belkin et al., 1986). We have studied the fluid inclusions and mineral chemistry of the authigenic assemblage of anhydrite and phlogopite. Anhydrite is becoming increasingly recognized as an important physicochemical indicator in geothermal and mineralized hydrothermal systems (e.g., Cavarretta et al., 1982; Queen and Motyka, 1984; Hattori et al., 1985). Authigenic phlogopite in geothermal or hydrothermal systems is rare; furthermore, fluid-inclusion studies of phlogopite are unknown to the authors. Therefore, we have also undertaken extensive microprobe analyses of the phlogopite mineral chemistry as a function of sample depth and crystal zoning. Phlogopite reflects the relative fugacities of HF, HCl, O_2, H_2, and water during crystallization and hence monitors intensive variables during hydrothermal processes. The detailed characterization of the SH2 authigenic phlogopite is especially important because we can define its environment of formation in terms of pressure, temperature, and fluid composition. The trace-element chemistry of the authigenic anhydrite was also determined in an attempt to provide additional information on the nature of the coexisting solutions.

Geologic setting

The Sabatini volcanic district is part of the perpotassic Roman comagmatic province of Washington (1906) that borders the eastern Tyrrhenian Sea and is aligned along a NW-SE tectonic trend. Although the origin of the volcanic activity is debated, the most current interpretation defines the tectonic style as postcollisional and the associated magmatism as subduction related rather than resulting from intraplate rifting (e.g., Di Girolamo, 1978; Rogers et al., 1985).

The largest volcano-tectonic structure in the area, an almost square depression, is located near the Bracciano village and is now a lake (Bracciano Lake). The Sacrofano center, a stratovolcanic structure, is the main eruptive center (De Rita et al., 1983). Numerous other minor centers (~20) give the area a "crater-field" morphology. Their activity was mainly explosive, producing huge volumes of pyroclastics; lava flows, very subordinate in volume,

are most abundant in the northern part of the Bracciano Lake area. The lake perimeter is characterized by several recent minor eruptive centers, such as Trevignano, Vigna di Valle, Polline, and Acquerello.

The oldest dated products of the Sabatini complex are the 0.6 Ma Morlupo center pyroclastics, whereas the youngest dated product is the 0.083 Ma Baccano pyroclastic flow. However, as defined by stratigraphy, the latest products were erupted from the Martignano, Le Case, and Stracciacappe centers (Di Filippo et al., 1984).

The composition of products erupted within the Sabatini volcanic district is considered to be transitional between the mafic Alban Hills leucitites (to the south) and the differentiated Vico and Vulsini suites (to the north). The Sabatini lavas have been discussed in detail by Cundari (1979) who showed that the lavas cluster in the tephritic leucite phonolite and tephritic leucitite fields of the Streckeisen "APF" diagram. The compositional variations of the lavas are related to crystal-liquid differentiation in a subvolcanic (low-pressure) regime (Cundari, 1979).

The volcanic rocks lie on a sedimentary basement whose stratigraphy has been reconstructed by Baldi et al. (1974) for the northern Roman Region and by Funiciello and Parotto (1978), who provided additional data and extended the reconstruction to southern Latium. From the above studies the stratigraphy of the sedimentary basement of the area is as follows: (1) an upper allochthonous flyschoid complex (Late Cretaceous to Oligocene-Miocene) that varies from alternating calcarenites, marly limestones, and clays to alternating calcarenites and quartzo-feldspathic sandstones (200 to 1000 m in thickness) and (2) a lower carbonate basal complex (oldest dated as Late Triassic) that consists of marls, marly limestones, and limestones with a marly limestone that contains alternating dolomitic layers with minor anhydrite layers in the lower section (total thickness of complex can be 2000 m).

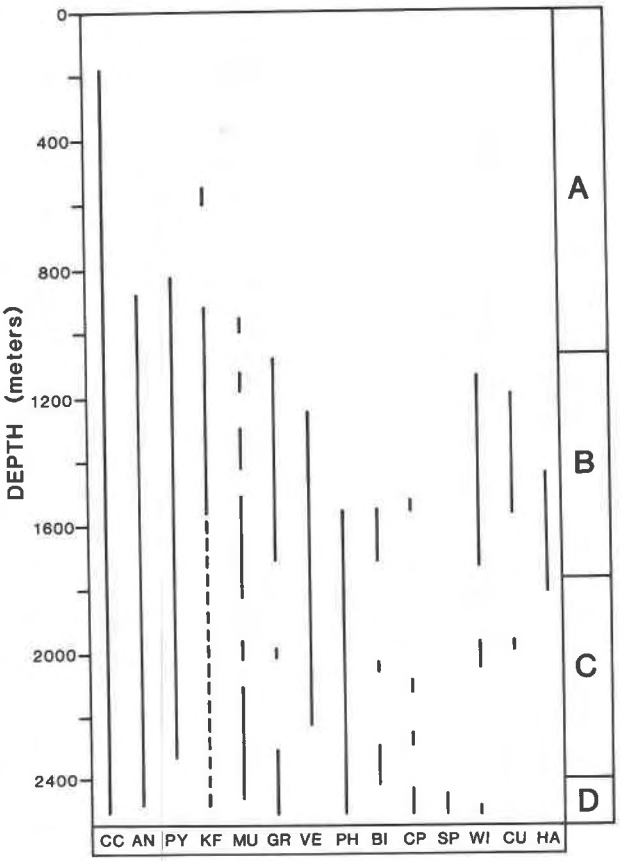

Fig. 2. Distribution of the major newly formed minerals as a function of depth in the SH2 well from Cavarretta and Tecce (1987). CC = calcite, AN = anhydrite, PY = pyrite, KF = K-feldspar, MU = K-mica and/or sericite, GR = garnet, VE = vesuvianite, PH = phlogopite, BI = biotite, CP = clinopyroxene, SP = spinel, WI = wilkeite, CU = cuspidine, HA = harkerite. Also shown are the four zones as distinguished by Cavarretta and Tecce (1987). A = chlorite ± zeolite zone; B = K-feldspar ± garnet (grandite) ± vesuvianite ± wilkeite ± cuspidine ± harkerite zone; C = vesuvianite ± phlogopite zone; D = phlogopite ± pyroxene ± spinel zone.

Samples studied

The stratigraphy and hydrothermal mineral distribution of the SH2 well as reported by Cavarretta and Tecce (1987) can be summarized as follows: Above 460 m, the well penetrated various volcanic products—lava and pyroclastic flows (phonolites, leucitites, and leucitic tephrites) and volcaniclastic breccias. Chlorite, calcite, and zeolites (mostly phillipsite) are present as glass alteration or newly formed minerals. Below 460 m the well entered the allochthonous flyschoid complex, which was significantly recrystallized below 1070 m. Samples of the so-called "Cicerchina," a facies of the flyschoid complex, are distinctly present between 1450 and 1560 m. Below 1560 m the original rock type is not recognizable, and the presence of the "carbonate basal complex" is assumed. From 1070 m to the bottom of the well at 2498.7 m, authigenic minerals are particularly abundant and mark the top of the "contact metasomatic complex" defined by the first appearance of garnet. Figure 2 shows the distribution of the major authigenic phases as a function of depth.

Cavarretta and Tecce (1987; see Fig. 2) have defined four main zones of hydrothermal minerals (calcite is ubiquitous below 180 m, as are anhydrite and pyrite below 870 m): (A) a near-surface chlorite ± zeolite domain in the volcaniclastic units, (B) a K-feldspar ± garnet (grandite) ± vesuvianite ± wilkeite ± cuspidine ± harkerite ± wollastonite ± apatite domain in the top part of the "contact metasomatic complex," (C) a vesuvianite ± phlogopite domain in the midpart of the same complex, and (D) a phlogopite ± pyroxene ± spinel ± cancrinite domain in the bottom part.

All the phlogopite samples and all the anhydrite samples except the core at 2168 m were selected from drill-cuttings. The estimated positional uncertainty of the drill-cutting samples is ±2 m.

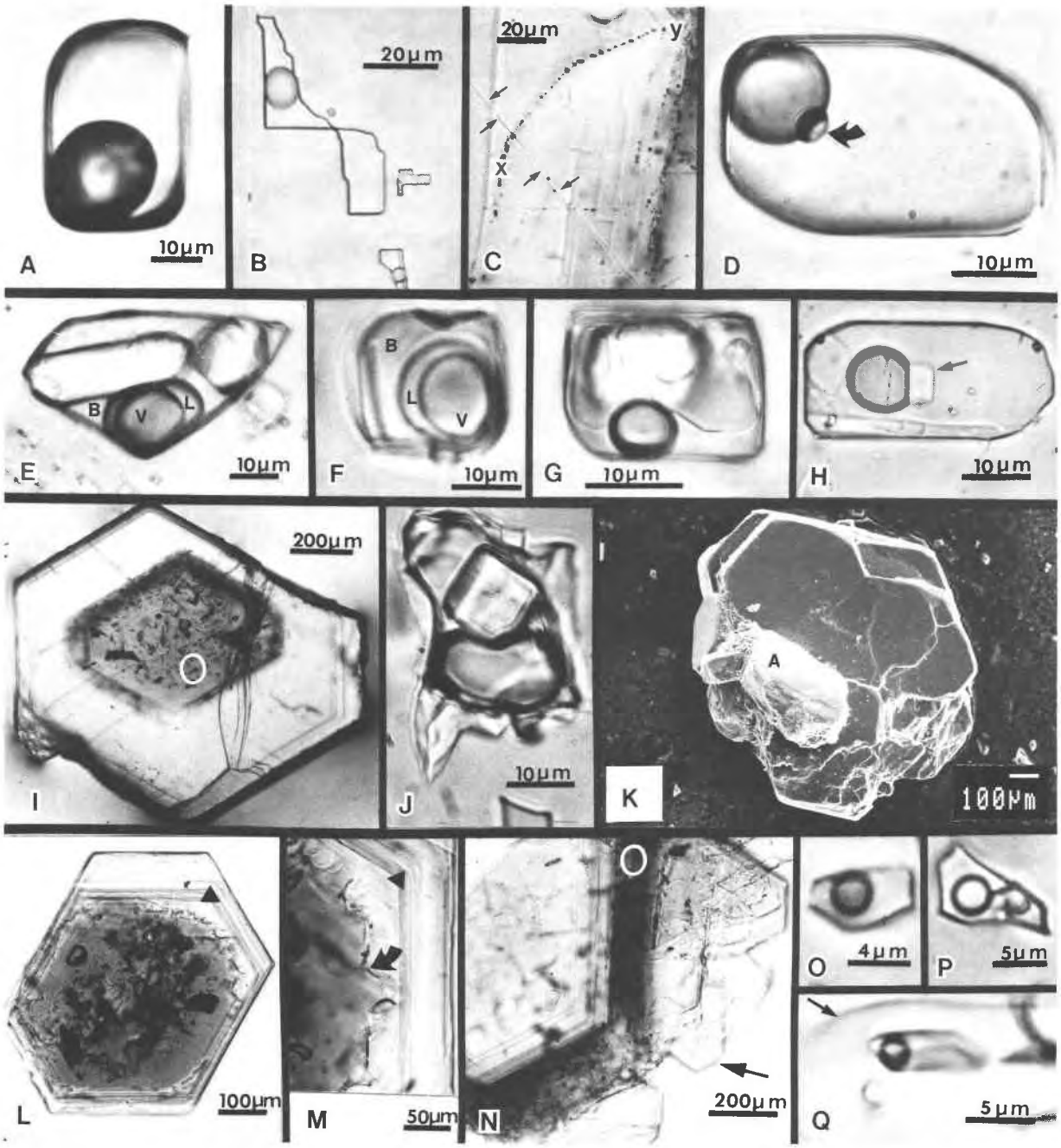

Fig. 3. (**A**) Primary two-phase (V + L) inclusion in anhydrite from sample 2210 m, the third dimension is ~35 μm. (**B**) Two-phase inclusion in anhydrite from 2040 m. The inclusion is necked-down, and further recrystallization would separate the parts. A small single-phase (L) inclusion suggests that this process is a low-temperature one. The inclusions are flattened in the {010} plane. (**C**) An example of a curvilinear plane (*X*-*Y*) of secondary (or pseudosecondary?) two-phase inclusions in anhydrite from 2150 m. The arrows indicate the common {011} twin plane. (**D**) A primary three-phase inclusion in anhydrite from 2040 m. The arrow points to an immiscible liquid phase that is preferentially wetting the vapor bubble. (**E**) A primary multiphase inclusion in anhydrite from 2168 m. Two immiscible liquids are present: brine (B) and CO_2 (confirmed by laser Raman spectroscopy) with liquid CO_2 (L) preferentially wetting the vapor bubble (V). The L + V CO_2 homogenized in the vapor phase at +28.3 °C. (**F**) A primary three-phase inclusion in anhydrite from 2040 m. Two immiscible liquids are present; brine (B) and liquid hydrocarbon (L) preferentially wetting the vapor bubble (V). The L and V phases homogenize at +32.9 °C in the vapor phase. (**G**) A primary multiphase inclusion in anhydrite from 1600 m photographed with partially crossed polarizers. Four included crystals appear isotropic although some are very thin (~3 to 4 μm). Two are birefringent. (**H**) A primary multiphase inclusion in anhydrite from 2150 m. The bubble is preferentially wetting a slightly pleochroic crystal (arrow) that may be a mica. (**I**) A zoned crystal of

The anhydrite and associated calcite, when observed in core, occupy common vein and pore-space fillings. Phlogopite occurs intergrown with anhydrite (Fig. 3K) in both core and drill-cuttings. The evidence for the hydrothermal origin of phlogopite is based on this textural relationship and the fluid-inclusion and chemical data discussed below.

Fluid inclusions

Fluid inclusions have been studied in hydrothermally formed anhydrite and phlogopite throughout the SH2 deep well in order to better understand the physicochemical characteristics of the fluid at the time of trapping, its origin, and possible evolution. Although fluid inclusions were observed in other authigenic phases, only in phlogopite and especially anhydrite was their abundance and distribution sufficient for a systematic study. In three cases the temperature of homogenization was determined for primary fluid inclusions in apatite crystals trapped in phlogopite crystals.

Fluid inclusions in micas have been rarely studied (Roedder, 1984). However, Pomârleanu and Sabliovschi (1980) reported primary fluid inclusions in muscovite with temperatures of homogenization (T_h) that vary from 220 to 600 °C. Trapping of fluid as a result of twinning on growth boundaries (twinning sutures) during fluorphlogopite synthesis has also been noted by Kozlova et al. (1984).

Methods

Microthermometry was performed with a USGS design and CHAIXMECA heating and freezing stages at the University of Rome and the U.S. Geological Survey, Reston. The stages were independently calibrated using organic and inorganic compounds as described by Roedder (1984). The instrumental uncertainty was estimated to be $\sim \pm 0.1$ °C in the range of the final melting point of ice (T_m) and $\sim \pm 2.0$ °C in the heating mode. The samples were heated only once to avoid spurious measurements that might be due to possible stretching or decrepitation.

Unpolished broken fragments (1–3 mm) of anhydrite crystals and small (0.5–2 mm) euhedral to subhedral phlogopite crystals were used. This lack of sample preparation (i.e., no doubly-polished plates) undoubtedly helped preserve fluid inclusions that otherwise might have been removed or partially decrepitated. We judge that sample preparation probably would have decrepitated or partially decrepitated all fluid inclusions in phlogopite.

The crushing-stage technique (Roedder, 1970) was used on anhydrite in order to obtain a qualitative estimate of the presence and composition of noncondensable gases. The crushing media was immersion oil or an aqueous alkaline $BaCl_2$ solution.

Description of fluid inclusions in anhydrite

Three different inclusion types were distinguished. Type A inclusions (Fig. 3A) are two-phase (L + V) liquid-rich aqueous inclusions with variable salinity. These are the most common and were used for the heating and freezing measurements. Type A inclusions are both primary and secondary (pseudosecondary?). Primary type A inclusions (Fig. 3A) typically are larger than secondary type A inclusions and have an equant shape. Type A secondary (pseudosecondary?) inclusions (Fig. 3C) commonly occupy curvilinear planes, are smaller, and tend to be flattened in the (010) plane. The correspondence between microthermometric data (see below) of the primary and secondary type A inclusions suggests that the latter may be pseudosecondary, but we have no supporting petrographic evidence.

Type B inclusions are monophase, either liquid or vapor, primary or secondary inclusions. Occasionally, we observe these inclusions to be the result of a necking-down process. Figure 3B shows that the necking-down process can produce monophase liquid inclusions. Necking can also produce monophase vapor inclusions. However, we also observe isolated monophase vapor inclusions. Crushing experiments (see below) have revealed the presence of noncondensable gases at pressures greater than 1 atm. Fracturing induced by the drilling process could produce monophase vapor inclusions that are caused by the expansion of gases during decompression on ascent with the resultant expulsion of liquid.

Type C inclusions are primary, multiphase, and liquid-rich. Inclusions of this type are uncommon, and their assemblages are varied. The most common type C assemblage (Fig. 3G and 3H) comprises vapor, liquid, plus one or more crystal phases. The crystal phases are birefringent or nonbirefringent and euhedral to anhedral. In a few

---

phlogopite from 2210 m. The core contains numerous fluid inclusions (one in white oval, shown in Fig. 3J) and is separated from a relatively inclusion-free zone by a sharp boundary. (**J**) A primary three-phase inclusion from the core of a phlogopite crystal (white oval, Fig. 3I). The included crystal is birefringent and appears to be anhydrite. (**K**) A crystal of phlogopite, imaged in secondary-electron emission by a JEOL JMS-840SEM, from 2210 m. A crystal of anhydrite (A) identified by SEM energy-dispersive analysis is partially enclosed by the phlogopite crystal. (**L**) A zoned crystal of phlogopite with a darker, inclusion-rich core separated from the lighter outer portion by an irregularly scalloped dissolution boundary. (**M**) An enlargement of an area from Fig. 3L; the solid triangle is in the same location in both Fig. 3L and Fig. 3M. The details of the scalloped dissolution boundary (arrow) are shown. (**N**) A zoned crystal of phlogopite from 2210 m. The upper left is a portion of the lighter-colored core. This is enclosed by a darker-colored zone (white oval) that is in turn surrounded by a faceted irregular rim (arrow). The darker zone is inclusion-rich although the inner core also contains both solid and fluid inclusions. (**O**) A primary two-phase inclusion from the dark zone of Fig. 3N (white oval). (**P**) A primary multiphase inclusion from the dark zone of Fig. 3N (white oval). (**Q**) A primary two-phase inclusion in a corroded apatite needle from the core of Fig. 3N. The arrow points to the curved phlogopite-apatite boundary with the arrow on the phlogopite side.

cases we can identify these crystal phases as daughter crystals (Roedder, 1984).

An uncommon type C assemblage (Figs. 3D and 3F) comprises two immiscible liquids plus vapor. Some of these multiphase inclusions were identified as containing liquid CO_2, and others, liquid hydrocarbon(?). Figure 3D shows a small globule preferentially wetting the vapor bubble. This phenomenon was observed in a group of primary inclusions, which suggests that this is a primary fluid component and not the result of later contamination (e.g., drilling fluids). Figure 3F shows a similar assemblage. This inclusion did not appear to absorb infrared, and the vapor and adjacent liquid phase homogenized at +32.9 °C in the vapor phase. This suggests that it is not vapor and liquid CO_2. However, some type C inclusions contain immiscible fluids that appear to be liquid and vapor CO_2 (confirmed by laser Raman spectroscopy, see below). Figure 3E shows an inclusion where the vapor and adjacent liquid homogenized at +28.3 °C and was an excellent absorber of infrared and hence is presumed to be CO_2. Figure 3E also shows the presence of solid phases that are probably accidentally trapped crystals.

Figure 3H shows a solid phase (daughter?) that is preferentially wetted on its apparent basal surface by the vapor bubble. This phenomenon is similar to that described by Roedder (1984) and Belkin et al. (1985) for mica.

Description of fluid inclusions in phlogopite

Two different types of fluid inclusions were observed in phlogopite . Type A inclusions (Fig. 3O) are two-phase (L + V), liquid-rich, and aqueous. Both primary and secondary (pseudosecondary?) type A inclusions were recognized. The primary inclusions were most commonly found in the darker phlogopite zones (Fig. 3N) and were usually isolated. We believe they are primary on the basis of the following criteria: (1) they are always concentrated in the darker zones regardless of the sequence of zoning (e.g., dark rim and light core or light rim and dark core); we do not believe that the dark-zone preference that the fluid inclusions show is the result of a difference in solubility between the light and dark zones acting on a healing fracture (Roedder, 1969), and (2) they sometimes occur along with solid inclusions outlining growth planes, as distinguished by color zoning.

Only the small (<35 μm) inclusions were usable for heating and freezing measurements. Larger inclusions obviously leaked as also did some small ones. Secondary (pseudosecondary?) type A inclusions were distributed along healed fractures parallel to (001) that cut across zoning.

Type B inclusions (Figs. 3J and 3P) are multiphase (L + V + solid), liquid-rich, and aqueous with one or more birefringent or nonbirefringent, euhedral to anhedral solid phases. Most trapped crystals were isolated occurrences and did not melt during heating; hence they are probably accidentally trapped crystals. In a few cases, groups of type B inclusions were observed, all containing the same solid and fluid phase assemblages and proportions relative to the inclusion volume. Although these crystals were only partially melted at vapor-liquid homogenization, they are considered to be daughter crystals. Many large (>50 μm) inclusions contained crystals but decrepitated upon heating. In many cases the crystals appeared to be cubic and hence looked like halite (Fig. 3J), but all were birefringent and probably are anhydrite.

We did not observe any inclusions with two immiscible liquids in phlogopite . Furthermore, we recognize that the population of inclusions on which we obtained heating and freezing data are biased. We observed that many inclusions in anhydrite, when crushed, yielded gas under pressure greater than 1 atm. We also noticed that many fluid inclusions in phlogopite, even small ones, decrepitated along the weak (001) cleavage when heated. This biases the data toward those inclusions containing small amounts of (or no) noncondensable gases.

Small, usually corroded, elongate crystals of apatite were commonly observed in the phlogopites. They were identified as apatite by optical properties and by SEM energy-dispersive analysis on exposed crystals. In three cases the apatite crystals contained primary type A fluid inclusions (Fig. 3Q) that were amenable to vapor-liquid homogenization measurement.

Microthermometry results

Pressure correction

A pressure correction (Potter, 1977) appropriate for the estimated trapping pressure and salinity was applied to all the T_h data subsequently discussed. The correction was calculated with the following assumptions: (1) the present water table of −50 m existed at the time of trapping, (2) the pressure was hydrostatic, and (3) the thermal gradient at the time of trapping was similar to the one now present in the well. A step-wise integration of the liquid densities from Keenan et al. (1969) and Potter and Brown (1977) was used with the water P-T data from Fisher (1976). The correction for both phlogopite and anhydrite T_h data ranged from +8 to +14 °C. Thus, the data presented on Figures 4 and 6 are trapping temperatures (T_t).

Anhydrite microthermometry data

To observe any phase changes upon warming, 188 primary and 28 secondary type A and C inclusions were frozen (Fig. 5), and 276 primary and 67 secondary type A and C inclusions were heated to vapor-liquid homogenization (Fig. 4).

On warming frozen inclusions, the eutectic temperature (T_e) of the phase assemblage was detectable; however, the small size or poor optical quality of the inclusions prevented this observation in most inclusions. When observed, most T_e values were ~−27 °C although a few ranged from −25 °C to −20 °C. In two cases we observed T_e to be ~−50 °C. Although the fluid composition probably lies in the system containing Ca and Na with T_e = −52 °C (Crawford, 1981), apparently the Ca species is at

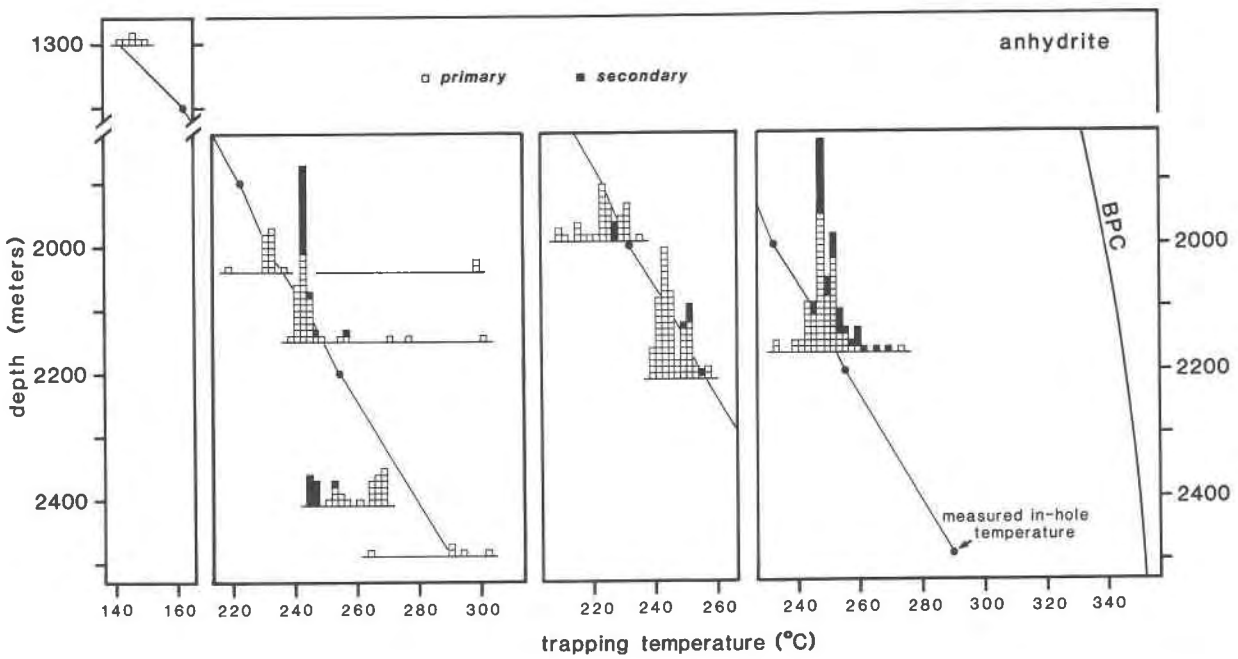

Fig. 4. The temperature of trapping (T_t) data for primary and secondary fluid inclusions in SH2 anhydrite as a function of sample depth (m). The T_h data have been pressure corrected as described in the text. Also shown are the measured in-hole temperatures, and the boiling-point curve (BPC) for pure water (Haas, 1971) adjusted for a water table of −50 m. Samples from 1990, 2168, and 2210 m have been offset to the right to avoid overlap. The in-hole temperatures were measured in stabilized conditions to minimize the effect of external interferences. The uncertainty in the in-hole temperature measurement is ±1–2 °C in the range 140–200 °C and ±2–5 °C in the range 200–300 °C.

such a low concentration that the T_e melting at low temperature (~ −50 °C) was insufficient to observe routinely.

Upon further warming, the temperature of the last melting of ice (T_m ice) was generally observable. Values for T_m ice (vapor-present) for primary inclusions ranged from −0.3 to −10.0 °C with most between −0.3 and −3.0 °C. We have recast the T_m ice data into weight percent NaCl equivalent assuming the dominance of NaCl as the dissolved species. Figure 5 shows the intra- and intersample variability of the salinity data. The salinity ranges from ~0.5 to 14 wt% NaCl equivalent. Upon freezing, a few two-phase (L + V) inclusions yielded a solid that persisted above 0.0 °C. The melting point of these presumed gas clathrates ranged from +1.55 to +20.0 °C. Since CO_2 clathrates are unstable above ~+10 °C (Collins, 1979), the higher T_m ice values indicate that other gases (hydrocarbons) must be present. Clathrate formation was recognized from all sample depths. However, CO_2 as a solute can depress the freezing point by a maximum of −1.48 °C without forming clathrate (Hedenquist and Henley, 1985). Hence, we cannot distinguish between the effects of dissolved salts or CO_2 in some low-salinity inclusions in anhydrite and phlogopite.

A small number of secondary inclusions were frozen and yielded T_m ice that ranged from −0.4 to −3.9 °C. The salinity for these inclusions ranged from 0.7 to 6.3 wt% NaCl equivalent.

All primary and secondary type A inclusions homogenized to a fluid by the disappearance of the vapor phase upon heating. The T_t values of primary and secondary type A inclusions were similar except for a sample from 2410 m where the secondary inclusions had T_t values ~20 °C less than the average for primary inclusions. The T_t values for primary type A inclusions ranged from ~140 °C at 1300 m to ~320 °C at 2490 m.

Heating type C inclusions revealed that some included crystals dissolve below vapor-liquid homogenization and some remained unaffected.

Figure 4 shows that the mode of all the pressure-corrected T_h data for each sample except for those from 2410 m falls within ±10 °C of the measured in-hole temperature. This agreement is very good considering the limitations and assumptions of the data.

Phlogopite microthermometry data

Ninety primary type A and B inclusions were heated to vapor-liquid homogenization (Fig. 6), and 79 were frozen to observe any phase changes upon warming (Fig. 7). After freezing, the inclusions were slowly warmed in an attempt to determinate T_e. The T_e was −45 ± 5 °C but was difficult to observe at best. The determination of T_m ice was easier because of better resolution of the remaining ice crystals. In only one inclusion from sample 2480 m was evidence of clathrate ice (T_m = +9 °C) observed. Figure 7 shows the T_m ice data recast into weight percent NaCl equivalent. The salinity ranged from 0.2 to 7.8 wt%

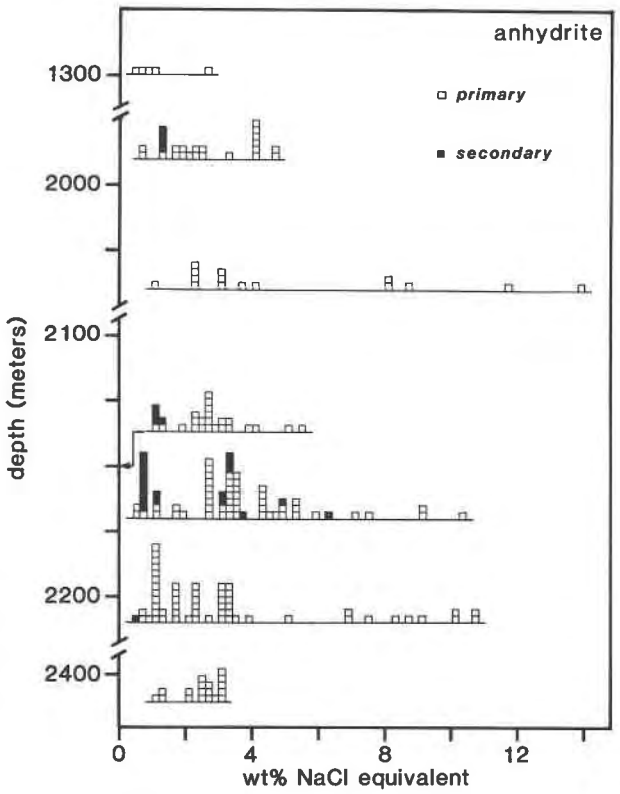

Fig. 5. The salinity (wt% NaCl equivalent) data for primary and secondary fluid inclusions in SH2 anhydrite as a function of sample depth (m).

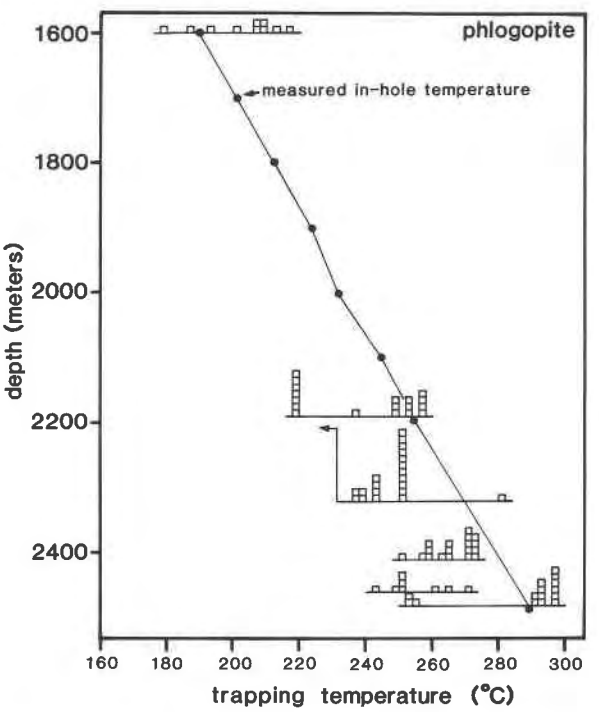

Fig. 6. The temperature of trapping (T_t) data for primary fluid inclusions in SH2 phlogopite as a function of sample depth (m). The T_h data have been pressure corrected as described in the text. Also shown are the measured in-hole temperatures. The sample from 2210 m has been offset to avoid overlap.

NaCl equivalent with a considerable scatter and was similar to that shown by the anhydrite data.

Type A and type B inclusions were heated, and all homogenization to fluid was by the disappearance of the vapor phase. Over 50% of the heated inclusions decrepitated before vapor-liquid homogenization. This suggests the presence of dissolved gases. No included crystals were seen to melt before vapor-liquid homogenization, although one group became noticeably rounded.

T_t ranged from 178 °C at 1600 m to 298 °C at 2480 m. Figure 6 shows that although the data are limited, there is a definite increase of T_t with depth. Three two-phase primary fluid inclusions in apatite (Fig. 3Q) homogenized to liquid at 250 °C from sample 2210 m. This temperature is similar to that of the inclusions in the host phlogopite .

Crushing data

Selected anhydrite crystals from all samples were crushed in oil. The good cleavage of anhydrite and the mode of occurrence of the fluid inclusions in groups made this technique difficult. Evolution of gas, at a pressure greater than atmospheric, was noted in all samples but only in some inclusions. The vapor bubbles expanded various amounts from just filling the inclusion volume to evolving bubbles into the crushing medium. This was observed in both primary and secondary inclusions. A few crushing runs in an alkaline $BaCl_2$ solution revealed the faint presence of a white precipitate ($BaCO_3$) after sudden bubble collapse, confirming the presence of CO_2 as a volatile component.

Laser Raman spectroscopy

Limited laser Raman spectroscopic analyses were performed on one multiphase (Fig. 3E) and six two-phase inclusions in anhydrite. The technique used was similar to that described by Dhamelincourt et al. (1979). The analyses confirm the presence of CO_2 in the multiphase inclusion and indicate the absence of noncondensable gases (CO_2, H_2S, CO, and N_2) in the six two-phase inclusions. This latter result supports the observations, made by crushing and petrography, of a variable presence of noncondensable gases in the fluid inclusions of the SH2 anhydrites.

Phlogopite mineral chemistry

Analytical method

Small (0.5–2 mm) euhedral to subhedral phlogopite crystals were handpicked, where present, from the drill-cuttings. Only those crystals that contained primary fluid inclusions were selected. A standard petrographic slide was frosted on one side with 800 grit Al_2O_3 abrasive and then cleaned and dried. A very thin layer of clear epoxy (e.g., Devcon 2-Ton) was applied with the edge of a razor blade. Under a low-power binocular micro-

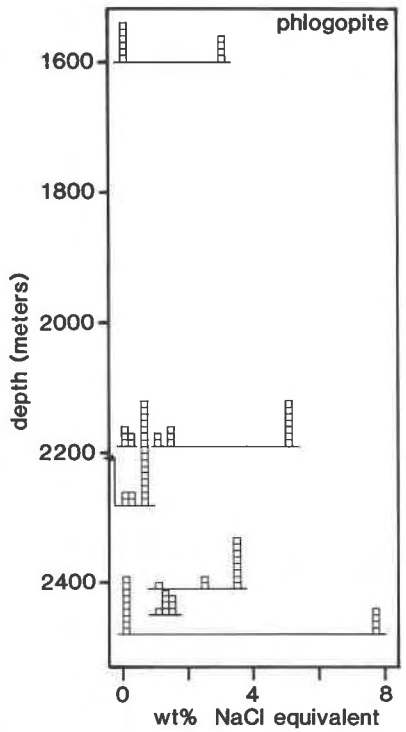

Fig. 7. The salinity (wt% NaCl equivalent) data for primary fluid inclusions in SH2 phlogopite as a function of sample depth (m).

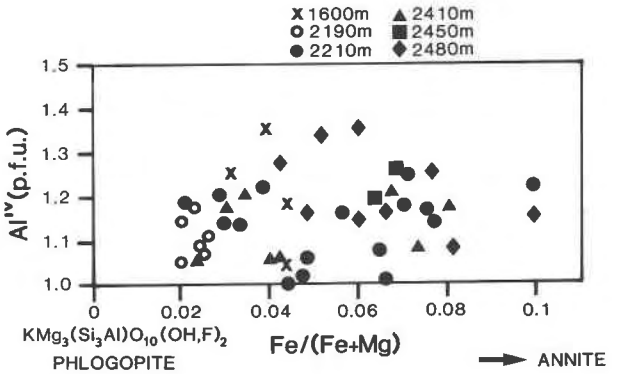

Fig. 8. Variation of the phlogopite composition from the SH2 well as a function of two coupled substitutions (based on an 11-oxygen-equivalent normalization). The abscissa shows the substitution $Mg^{2+} \rightleftharpoons Fe^{2+}$, phlogopite to annite, as expressed by Fe/(Fe + Mg), Fe = total Fe by microprobe. The ordinate shows the substitution $^{[6]}(M^{2+}) + {}^{[4]}(Si^{4+}) \rightleftharpoons {}^{[6]}(Al^{3+}) + {}^{[4]}(Al^{3+})$ as expressed by the variation in $^{[4]}Al$ per formula unit (pfu). All the phlogopite data presented in Figs. 8–10 and 12–16 represent the complete population of microprobe analyses (Table 1). The light and dark zones in single crystals are plotted as separate points. Only in Fig. 9 are these points paired and marked with respect to their relative color.

scope, the separated crystals were arranged in a recorded pattern, then set aside for the epoxy to cure (1 h). The epoxy must be exceedingly thin in order to allow the single crystals to be gently pushed against the slide without the epoxy flowing up and over their top surfaces. After curing, cleaning, and C-coating, the crystals were examined with reflected-light optics to distinguish those areas on the (001) surface that were perfectly flat, smooth, and suitable for electron-microprobe analysis.

The phlogopite crystals are commonly zoned when viewed perpendicular to (001). Any analysis from any other direction in a zoned crystal would give values that may or may not be meaningful in terms of the systematic element distribution of the zoning.

An ARL-SEMQ electron microprobe with four fixed and four driven spectrometers was used for wavelength-dispersive analysis. Operating conditions were 15-kV voltage and a 0.1-μA beam current. Standardization was done before each analytical session on silicates of known composition, similar structure, and element abundances similar to those anticipated in the phlogopites. Selected representative analyses are given in Table 1. Table 1 also gives the standard deviation (1σ) and the detection limit associated with each element. The count data were reduced on-line by a Bence-Albee scheme as adapted by McGee (1983). The background interpolation method of M. Mangan (pers. comm., 1985) was used. Each analysis reported in Table 1 represents the average of 3 to 9 individual analyses on different 10-μm beam spots. Phlogopite analyses of crystals from any given sample were always run during different analytical sessions to avoid any systematic error associated with any one analytical session.

The crystallography of a phlogopite crystal from 2210 m was determined by the precession technique, and the results are given in Appendix 1.

Normalization procedure

Microprobe analysis cannot distinguish bewteen Fe^{2+} and Fe^{3+}, and the H_2O in hydrous silicates is not determined. We have used the program and normalization scheme of Flohr (1983) that involves normalization to 11 oxygen equivalents, i.e., total cation charge = 22. We have assumed that no Fe^{3+} is present. Hence, all Fe discussed subsequently is total Fe expressed as FeO. Table 1 gives the formula proportions using the above scheme. The OH was calculated by the method of Flohr (1983), assuming a full OH-site occupancy. We have also assumed that the substitution of O^{2-} for $(OH)^-$ does not occur. The cations are assigned to crystallographic sites for the stoichiometry $(^{[12]}\square, Na, Ca, K, Ba)(Fe, Mg, Mn, ^{[6]}Al, Ti, ^{[6]}\square)_3(^{[4]}Al, Si)_4O_{10}(OH,F,Cl)_2$ ($\square$ = vacancy). The vacancies are then calculated by difference.

Results

The SH2 phlogopite have nearly end-member compositions, with average Fe/(Fe + Mg) = 0.05, and vary in composition by two major cation substitution schemes. First, all the analyses are enriched in Al_2O_3, save two, compared to phlogopite-annite. The dominant mechanism causing Al enrichment in biotite involves the Al-Tschermak's substitution

$$^{[6]}(M^{2+}) + {}^{[4]}(Si^{4+}) \rightleftharpoons {}^{[6]}(Al^{3+}) + {}^{[4]}(Al^{3+}).$$

Figure 8 shows the variance of $^{[6]}(M^{2+})$ and $^{[4]}(Al^{3+})$. The values range from 1.0 to 1.35 $^{[4]}Al$ per 11 oxygens. The other cation substitution involves $Mg^{2+} \rightleftharpoons Fe^{2+}$; the phlogopite component ranges from 90 to 98%. Figure 9 shows the variance of Mg with Fe, and the data show a

TABLE 1. Representative microprobe analyses of zoned and unzoned phlogopites from the SH2 well

Depth (m):	1600				2190					
Sample:	1	2	3	4	1	2	3	4	5	6
Description:	zoned light core	unzoned	unzoned	unzoned	unzoned	unzoned	zoned light core	unzoned	unzoned	unzoned
Number of analyses:	6	6	9	6	6	3	6	3	6	6
SiO_2	40.10	36.13	41.44	38.06	40.73	40.78	40.76	41.34	38.93	39.62
Al_2O_3	15.93	18.57	13.79	17.00	13.31	14.59	13.88	13.37	13.60	14.20
FeO	2.08	1.73	2.09	1.44	1.21	1.25	1.19	0.99	0.99	1.17
MgO	26.19	23.89	25.59	25.12	26.54	26.57	26.75	26.82	26.79	27.61
CaO	n.d.	n.d.	n.d.	n.d.	n.d.	0.03	n.d.	n.d.	n.d.	n.d.
Na_2O	0.10	0.10	0.10	0.10	0.09	0.08	0.09	0.07	0.09	0.08
K_2O	10.36	9.23	10.10	9.66	10.12	9.92	10.04	10.04	9.64	10.26
TiO_2	0.08	0.36	0.16	0.17	0.15	0.16	0.20	0.16	0.15	0.15
MnO	0.10	0.08	0.09	0.07	0.04	0.04	0.05	0.04	n.d.	0.04
BaO	1.14	3.81	1.02	2.52	1.38	1.46	1.01	1.52	2.01	2.11
Cl	0.26	n.d.	n.d.	n.d.	n.d.	n.d.	0.19	0.19	n.d.	n.d.
F	3.35	2.95	3.46	3.32	4.21	3.90	3.90	3.56	3.69	3.87
Sum	99.69	96.85	97.84	97.82	97.78	98.78	98.06	97.91	95.89	99.11
$-Cl \equiv O$	0.07	0.00	0.00	0.00	0.00	0.00	0.05	0.05	0.00	0.00
$-F \equiv O$	1.41	1.24	1.46	1.40	1.77	1.64	1.64	1.50	1.55	1.63
Sum	98.21	95.61	96.38	96.06	96.00	97.14	96.37	96.35	94.34	97.48
H_2O (calc)*	2.61	2.70	2.57	2.58	2.17	2.38	2.30	2.46	2.34	2.37
Sum	100.82	98.30	98.95	98.64	98.17	99.52	98.67	98.82	96.67	99.85
Cations calculated on the basis of 11 oxygen equivalents, total Fe as FeO										
Si	2.818	2.645	2.952	2.747	2.930	2.889	2.908	2.951	2.856	2.826
$^{[4]}Al$	1.182	1.355	1.048	1.253	1.070	1.111	1.092	1.049	1.144	1.174
T site	4.000	4.000	4.000	4.000	4.000	4.000	4.000	4.000	4.000	4.000
$^{[6]}Al$	0.138	0.248	0.110	0.194	0.059	0.107	0.076	0.059	0.032	0.021
Fe^{2+}	0.122	0.106	0.125	0.087	0.073	0.074	0.071	0.059	0.061	0.070
Mg	2.743	2.607	2.717	2.702	2.845	2.805	2.844	2.853	2.929	2.935
Ti	0.004	0.020	0.009	0.009	0.008	0.009	0.011	0.009	0.008	0.008
Mn	0.006	0.005	0.005	0.004	0.002	0.002	0.003	0.002	0.000	0.002
M site	3.014	2.985	2.965	2.996	2.988	2.997	3.005	2.982	3.030	3.036
Ca	0.000	0.000	0.000	0.000	0.000	0.002	0.000	0.000	0.000	0.000
Na	0.014	0.014	0.014	0.014	0.013	0.011	0.012	0.010	0.013	0.011
K	0.929	0.862	0.918	0.890	0.929	0.896	0.914	0.914	0.902	0.934
Ba	0.031	0.109	0.028	0.071	0.039	0.041	0.028	0.043	0.058	0.059
A site	0.974	0.985	0.961	0.976	0.980	0.950	0.954	0.966	0.974	1.004
Σ cations	7.988	7.971	7.925	7.970	7.968	7.947	7.959	7.948	8.002	8.040
F	0.745	0.683	0.780	0.758	0.958	0.874	0.880	0.804	0.856	0.873
Cl	0.031	0.000	0.000	0.000	0.000	0.000	0.023	0.023	0.000	0.000
OH (calc.)*	1.224	1.317	1.220	1.242	1.042	1.126	1.097	1.173	1.144	1.127
Sum	2.000	2.000	2.000	2.000	2.000	2.000	2.000	2.000	2.000	2.000
Fe/(Fe + Mg)	0.043	0.039	0.044	0.031	0.025	0.026	0.024	0.020	0.020	0.023
F/(F + OH)	0.373	0.343	0.390	0.379	0.479	0.437	0.440	0.402	0.428	0.436

Note: The standard deviations (1σ, wt%) for 3 to 9 individual analyses are SiO_2 = 0.52, Al_2O_3 = 0.43, FeO = 0.20, MgO = 0.47, CaO = 0.01, Na_2O = 0.01, K_2O = 0.19, TiO_2 = 0.04, MnO = 0.02, BaO = 0.15, and F = 0.21. The average detection limits (wt%) for the microprobe configuration used are SiO_2 = 0.05, Al_2O_3 = 0.03, FeO = 0.06, MgO = 0.04, CaO = 0.03, Na_2O = 0.02, K_2O = 0.04, TiO_2 = 0.04, MnO = 0.04, BaO = 0.11, Cl = 0.10, and F = 0.08. n.d. = not detected.

* H_2O calculation is based on the assumption of full OH site occupancy (OH = 2.00 − F − Cl) and is only used as a check on analysis sums.

good agreement for the substitution $Mg^{2+} \rightleftharpoons Fe^{2+}$. Figure 10 shows the variation of Fe/(Fe + Mg) with sample depth. From 1600 m to 2190 m there is a slight decrease in Fe/(Fe + Mg), then the average ratio increases. This picture is complicated by the fact that zoning also becomes more prevalent at depths below 2210 m.

Other elements analyzed for are Mn, Ti, K, Ba, Ca, Na, Cl, and F. The MnO contents vary from below the detection limit to 0.26 wt%. However, it clearly varies by the substitution $2\ Mg^{2+} \rightleftharpoons Fe^{2+} + Mn^{2+}$ (e.g., Fig. 11).

CaO was usually below the detection limit. Na_2O was always minor and varies from near the detection limit to 0.19 wt%. Cl was always at or below the detection limit. Volfinger et al. (1985) indicated that the Cl content of phlogopite is one-twentieth that of biotites. The dimension of the (OH,Cl) site, hence its occupancy, is mainly controlled by the rotation angle (α) of the tetrahedra, which is a direct function of the X_{Fe} in the biotite. Four phlogopite crystals were analyzed for Cr_2O_3. The Cr_2O_3 content was found to be at or below the detection limit (0.03 wt%). Ti, K, Ba, and F variations are discussed below.

Phlogopite color and zoning. The SH2 phlogopites, when viewed perpendicular to (001), display variation in color from colorless to very dark green, which is in part a function of crystal thickness. Very striking, especially in small (~2 mm) euhedral to subhedral crystals, is a simple but sharp light and dark zoning (Fig. 3I). As either the core or the rim can be light or dark, the color is probably a

TABLE 1—*Continued*

2210											
1 zoned light rim	1 zoned dark core	2 zoned dark rim	2 zoned light core	3 zoned dark core	4 zoned light rim	5 zoned light rim	5 zoned dark core	6 zoned light rim	6 zoned dark core	7 zoned light rim	7 zoned dark core
3	3	3	3	6	6	4	3	9	3	3	3
39.99	40.00	40.47	41.51	40.40	39.65	38.80	40.96	39.84	38.04	38.64	39.16
14.60	15.04	13.93	12.95	13.88	15.00	14.43	11.83	13.73	15.02	15.41	15.22
1.07	3.52	2.92	2.53	3.02	1.56	1.36	3.38	1.47	4.74	1.85	3.53
28.42	26.38	27.50	28.25	24.74	25.85	27.41	26.78	27.29	24.18	26.58	24.35
n.d.	n.d.	n.d.	n.d.	n.d.	n.d.	n.d.	n.d.	n.d.	n.d.	n.d.	n.d.
0.05	0.04	0.04	0.05	0.13	0.07	0.08	0.08	0.07	0.07	0.07	0.07
9.99	10.17	10.30	10.45	10.02	9.85	10.43	11.01	10.70	10.45	10.72	10.53
0.13	0.28	0.35	0.17	0.25	0.18	0.23	0.15	0.19	0.53	0.19	0.26
n.d.	0.11	0.09	0.04	0.13	0.05	0.06	0.26	0.05	0.10	0.06	0.18
1.45	0.27	n.d.	n.d.	0.48	1.04	1.67	0.13	1.13	1.12	1.18	0.58
n.d.	n.d.	n.d.	n.d.	n.d.	n.d.	n.d.	n.d.	n.d.	n.d.	n.d.	0.22
4.42	3.73	4.40	4.57	3.52	4.68	3.33	3.58	4.22	3.33	3.53	3.41
100.12	99.54	100.00	100.52	96.57	97.93	97.80	98.16	98.69	97.58	98.23	97.51
0.00	0.00	0.00	0.00	0.00	0.00	0.00	0.00	0.00	0.00	0.00	0.06
1.86	1.57	1.85	1.92	1.48	1.97	1.40	1.51	1.78	1.40	1.49	1.44
98.26	97.97	98.15	98.60	95.09	95.96	96.40	96.65	96.99	96.18	96.74	96.02
2.16	2.48	2.17	2.12	2.47	1.94	2.59	2.48	2.16	2.53	2.51	2.47
100.42	100.45	100.32	100.71	97.56	97.90	98.99	99.13	99.16	98.71	99.25	98.49
Cations calculated on the basis of 11 oxygen equivalents, total Fe as FeO											
2.816	2.820	2.849	2.906	2.925	2.856	2.791	2.941	2.855	2.777	2.771	2.833
1.184	1.180	1.151	1.069	1.075	1.144	1.209	1.001	1.145	1.223	1.229	1.167
4.000	4.000	4.000	3.974	4.000	4.000	4.000	3.943	4.000	4.000	4.000	4.000
0.027	0.071	0.006	0.000	0.109	0.129	0.015	0.000	0.014	0.069	0.074	0.132
0.063	0.208	0.172	0.148	0.183	0.094	0.082	0.203	0.088	0.289	0.111	0.214
2.982	2.772	2.886	2.947	2.669	2.775	2.939	2.866	2.914	2.630	2.841	2.626
0.007	0.015	0.019	0.009	0.014	0.010	0.012	0.008	0.010	0.029	0.010	0.014
0.000	0.007	0.005	0.002	0.008	0.003	0.004	0.016	0.003	0.006	0.004	0.011
3.079	3.072	3.087	3.107	2.983	3.011	3.052	3.093	3.030	3.024	3.039	2.996
0.000	0.000	0.000	0.000	0.000	0.000	0.000	0.000	0.000	0.000	0.000	0.000
0.007	0.005	0.005	0.007	0.018	0.010	0.011	0.011	0.010	0.010	0.010	0.010
0.897	0.915	0.925	0.933	0.925	0.905	0.957	1.009	0.978	0.973	0.981	0.972
0.040	0.007	0.000	0.000	0.014	0.029	0.047	0.004	0.032	0.032	0.033	0.016
0.944	0.928	0.930	0.940	0.957	0.944	1.015	1.023	1.020	1.015	1.024	0.998
8.024	8.000	8.017	8.021	7.939	7.955	8.067	8.059	8.049	8.039	8.063	7.994
0.984	0.832	0.980	1.012	0.806	1.066	0.758	0.813	0.956	0.769	0.801	0.780
0.000	0.000	0.000	0.000	0.000	0.000	0.000	0.000	0.000	0.010	0.000	0.027
1.016	1.168	1.020	0.988	1.194	0.934	1.242	1.187	1.044	1.231	1.199	1.193
2.000	2.000	2.000	2.000	2.000	2.000	2.000	2.000	2.000	2.000	2.000	2.000
0.021	0.070	0.056	0.048	0.064	0.033	0.027	0.066	0.029	0.099	0.038	0.075
0.492	0.416	0.490	0.506	0.403	0.533	0.379	0.407	0.478	0.385	0.401	0.390

function of time of nucleation. In a few cases the phlogopites displayed more than this simple paired zoning. Figures 3N and 11 show euhedral crystals with three major zones. Superimposed on these major zones are very thin and compositionally subtle oscillatory zones. Detailed investigation of these oscillatory zones was not undertaken, but it appears that they result from changes in Fe^{2+}/Mg^{2+}. Also observed in a small number of phlogopite crystals is a dissolution texture always associated with the darker zones (Figs. 3L and 3M). In every case the dissolution event was followed by the crystallization of a lighter (Mg-rich) zone. The dissolution has occurred primarily on the edges of the phlogopite crystals and not on the (001) surface.

Phlogopite zoning is not common, and although there is considerable speculation as to the exact origin of the zoning, there is agreement that it is caused by some major perturbation in one or more intensive parameters (Rimšaite, 1969; Rashkova, 1981). Various mechanisms have been considered: (1) a change in the bulk composition of the precipitating fluid; (2) a change in pressure and/or temperature; (3) a preferential loss of H_2 during some event by which the solution becomes more oxidized, the activity of Fe^{2+} is lowered, and, hence, the phlogopites become enriched in Mg; and (4) that the Fe content varies as a function of growth rate. Baronnet and Velde (1977) have experimentally investigated the growth of phlogopite for constant chemical and physical parameters. They found

TABLE 1—*Continued*

Depth (m):	2210				2410					
Sample:	8	8	9	9	1	1	2	2	3	3
Description:	zoned light core	zoned dark rim	zoned light rim	zoned dark core	zoned light rim	zoned dark core	zoned light rim	zoned dark core	zoned dark core	zoned light rim
Number of analyses:	3	3	3	3	3	3	3	3	3	3
SiO_2	40.53	39.25	40.34	37.81	40.18	39.69	41.79	41.39	39.64	39.27
Al_2O_3	11.95	13.87	11.67	14.74	14.23	15.50	12.82	12.76	14.32	14.54
FeO	2.37	3.71	2.28	3.53	1.58	1.74	1.20	2.08	4.03	3.47
MgO	27.15	25.06	27.53	25.96	28.47	27.43	29.15	28.25	26.11	26.94
CaO	n.d.	n.d.	n.d.	n.d.	n.d.	n.d.	n.d.	n.d.	n.d.	n.d.
Na_2O	0.08	0.08	0.08	0.07	0.05	0.06	0.04	0.05	0.04	0.05
K_2O	11.02	10.80	10.84	10.75	10.26	10.00	10.57	10.33	10.11	9.80
TiO_2	0.20	0.30	0.17	0.24	0.16	0.16	0.15	0.11	0.40	0.41
MnO	0.08	0.12	0.08	0.16	n.d.	n.d.	n.d.	0.10	0.14	0.10
BaO	0.44	0.65	0.27	0.84	0.40	0.74	n.d.	0.37	n.d.	0.19
Cl	n.d.	n.d.	n.d.	0.16	n.d.	n.d.	n.d.	n.d.	n.d.	n.d.
F	3.57	3.24	5.00	3.79	4.29	4.06	4.58	4.56	4.14	4.05
Sum	97.39	97.08	98.26	98.05	99.62	99.38	100.30	100.00	98.93	98.82
$-Cl \equiv O$	0.00	0.00	0.00	0.04	0.00	0.00	0.00	0.00	0.00	0.00
$-F \equiv O$	1.50	1.36	2.11	1.60	1.81	1.71	1.93	1.92	1.74	1.71
Sum	95.89	95.72	96.16	96.41	97.81	97.67	98.37	98.08	97.21	97.12
H_2O (calc)*	2.46	2.59	1.76	2.28	2.23	2.33	2.13	2.10	2.24	2.29
Sum	98.35	98.30	97.92	98.69	100.04	100.00	100.50	100.18	99.44	99.40
Cations calculated on the basis of 11 oxygen equivalents, total Fe as FeO										
Si	2.928	2.854	2.926	2.753	2.828	2.797	2.915	2.914	2.829	2.798
$^{[4]}Al$	1.018	1.146	0.998	1.247	1.172	1.203	1.054	1.059	1.171	1.202
T site	3.945	4.000	3.923	4.00	4.000	4.000	3.969	3.974	4.000	4.000
$^{[6]}Al$	0.000	0.043	0.000	0.018	0.009	0.085	0.000	0.000	0.034	0.019
Fe^{2+}	0.143	0.226	0.138	0.215	0.093	0.103	0.070	0.122	0.241	0.207
Mg	2.923	2.716	2.976	2.817	2.987	2.881	3.030	2.965	2.777	2.861
Ti	0.011	0.016	0.009	0.013	0.008	0.008	0.008	0.006	0.021	0.022
Mn	0.005	0.007	0.005	0.010	0.000	0.000	0.000	0.006	0.008	0.006
M site	3.082	3.009	3.128	3.073	3.097	3.076	3.108	3.099	3.082	3.115
Ca	0.000	0.000	0.000	0.000	0.000	0.000	0.000	0.000	0.000	0.000
Na	0.011	0.011	0.011	0.010	0.007	0.008	0.005	0.007	0.006	0.007
K	1.016	1.002	1.003	0.999	0.921	0.899	0.941	0.928	0.921	0.891
Ba	0.012	0.019	0.008	0.024	0.011	0.020	0.000	0.010	0.000	0.005
A site	1.039	1.032	1.022	1.032	0.939	0.928	0.946	0.945	0.927	0.903
Σ cations	8.066	8.040	8.073	8.105	8.036	8.003	8.023	8.018	8.009	8.018
F	0.816	0.745	1.147	0.873	0.955	0.905	1.010	1.015	0.935	0.913
Cl	0.000	0.000	0.000	0.020	0.000	0.000	0.000	0.000	0.000	0.000
OH (calc.)*	1.184	1.255	0.853	1.108	1.045	1.095	0.990	0.985	1.065	1.087
Sum	2.000	2.000	2.000	2.000	2.000	2.000	2.000	2.000	2.000	2.000
Fe/(Fe + Mg)	0.047	0.077	0.044	0.071	0.030	0.034	0.023	0.040	0.080	0.067
F/(F + OH)	0.408	0.375	0.574	0.436	0.478	0.453	0.505	0.507	0.467	0.456

that increased growth rate increases the Fe and to a lesser extent the Ti content of the mica. The abundance of solid and fluid inclusions observed in the dark zones compared to the light zones also suggests that the dark zones grew more rapidly (Roedder, 1984).

Ba in SH2 phlogopites. The BaO content of SH2 phlogopite ranges from 0 to 3.8 wt% and can be enriched or depleted in similarly colored zones of the same or different crystals. Although the Ba content of SH2 phlogopite has scatter in any given sample, there appears to be a minimum in the average BaO content at 2410 m with increasing values at lesser and greater depths (Fig. 12). A similar variation in the Ba content of coexisting anhydrite is also seen (Fig. 12).

Ba^{2+} is nearly identical in size to K^+, and various substitutional schemes have been proposed: (1) $Ba^{2+} + {}^{[12]}\square \rightleftharpoons 2K^+$ (Shmakin, 1984) and (2) $Ba^{2+} + Al^{3+} \rightleftharpoons K^+ + Si^{4+}$ (Wentlandt, 1977). Figure 13 shows the variation of Ba^{2+} with K^+ and the position of the two substitutional schemes. The most statistically significant variation of Ba with K appears to behave according to scheme $Ba^{2+} + Al^{3+} \rightleftharpoons K^+ + Si^{4+}$. However, the displacements of the 1600-m and one of the 2210-m regression curves may indicate additional substitution into the interlayer site by other elements or vacancies.

The BaO content in relation to the obvious color zoning is complex. Figure 11 shows a zoned crystal where BaO in one zone can be either enriched or depleted relative to the other zone. Generally the darker (Fe-rich) zones have intermediate amounts whereas adjacent lighter zones have BaO contents that range from 0 to >3 wt%. The ratio of Ba-enriched to Ba-depleted adjacent light zones is approximately one. Although the data are limited, there does not appear to be any systematic difference between the Ba contents of light-colored centers or light-colored rims.

Ti in SH2 phlogopites. Ti in phlogopite is of interest

TABLE 1—*Continued*

2410		2450		2480							
4 zoned (very slightly) 3	5 zoned (very slightly) 3	1 zoned dark core 3	2 zoned (very slightly) 6	1 zoned (very slightly) 3	2 zoned dark core 3	3 zoned dark core 3	4 zoned dark core 3	5 zoned dark core 3	6 zoned light core 3	6 zoned dark rim 3	7 zoned dark core 3
41.09	40.17	37.94	38.82	39.42	39.48	39.52	37.80	36.55	35.79	40.33	39.26
13.40	13.32	17.42	16.23	15.53	16.21	14.94	17.37	18.48	17.48	13.19	13.59
2.05	3.47	3.12	2.88	3.08	2.20	2.81	3.38	2.31	2.72	3.81	4.82
26.07	24.61	23.87	23.90	24.47	24.24	24.60	23.09	23.94	24.07	24.42	24.56
n.d.	0.06	n.d.	n.d.	0.05	n.d.	n.d.	n.d.	n.d.	n.d.	n.d.	n.d.
0.08	0.19	0.10	0.16	0.11	0.08	0.08	0.08	0.09	0.08	0.06	0.06
9.83	10.25	9.78	9.65	10.67	10.46	10.55	10.19	10.10	9.68	10.79	10.71
0.30	0.49	0.22	0.39	0.25	0.20	0.29	0.23	0.27	0.28	0.89	0.86
0.08	0.14	0.07	0.07	0.09	0.05	0.10	0.11	0.05	0.08	0.11	0.13
0.93	0.45	1.96	1.28	0.84	0.98	0.54	1.84	2.30	2.97	0.34	0.27
n.d.	n.d.	n.d.	0.10	n.d.	n.d.	n.d.	n.d.	n.d.	n.d.	n.d.	n.d.
3.74	3.34	2.53	2.68	3.19	2.98	4.12	2.80	3.13	2.43	3.10	2.77
97.57	96.49	97.01	96.16	97.70	96.88	97.55	96.89	97.22	95.58	97.04	97.03
0.00	0.00	0.00	0.03	0.00	0.00	0.00	0.00	0.00	0.00	0.00	0.00
1.57	1.41	1.07	1.13	1.34	1.25	1.73	1.18	1.32	1.02	1.31	1.17
96.00	95.08	95.94	95.01	96.35	95.63	95.82	95.72	95.90	94.56	95.73	95.86
2.42	2.54	2.95	2.84	2.66	2.76	2.19	2.79	2.64	2.90	2.68	2.82
98.41	97.62	98.90	97.86	99.01	98.38	98.01	98.50	98.54	97.45	98.41	98.68
Cations calculated on the basis of 11 oxygen equivalents, total Fe as FeO											
2.941	2.921	2.739	2.812	2.832	2.837	2.860	2.748	2.657	2.650	2.917	2.849
1.059	1.079	1.261	1.188	1.168	1.163	1.140	1.252	1.343	1.350	1.083	1.151
4.000	4.000	4.000	4.000	4.000	4.000	4.000	4.000	4.000	4.000	4.000	4.000
0.072	0.062	0.222	0.198	0.148	0.210	0.134	0.237	0.242	0.176	0.042	0.011
0.123	0.211	0.188	0.174	0.185	0.132	0.170	0.206	0.140	0.168	0.230	0.293
2.781	2.667	2.568	2.580	2.620	2.596	2.653	2.502	2.594	2.656	2.632	2.656
0.016	0.027	0.012	0.021	0.014	0.011	0.016	0.013	0.015	0.016	0.048	0.047
0.005	0.009	0.004	0.004	0.005	0.003	0.006	0.007	0.003	0.005	0.007	0.008
2.996	2.975	2.994	2.979	2.972	2.952	2.979	2.964	2.994	3.021	2.960	3.015
0.000	0.005	0.000	0.000	0.004	0.000	0.000	0.000	0.000	0.000	0.000	0.000
0.011	0.027	0.014	0.022	0.015	0.011	0.011	0.011	0.013	0.011	0.008	0.008
0.898	0.951	0.901	0.892	0.978	0.959	0.974	0.945	0.937	0.914	0.996	0.991
0.026	0.013	0.055	0.036	0.024	0.028	0.015	0.052	0.066	0.086	0.010	0.008
0.935	0.995	0.970	0.950	1.021	0.997	1.001	1.009	1.015	1.012	1.014	1.007
7.931	7.970	7.964	7.929	7.993	7.950	7.980	7.972	8.009	8.032	7.973	8.022
0.847	0.768	0.578	0.614	0.725	0.677	0.943	0.644	0.720	0.569	0.709	0.636
0.000	0.000	0.000	0.012	0.000	0.000	0.000	0.000	0.000	0.000	0.000	0.000
1.153	1.232	1.422	1.374	1.275	1.323	1.057	1.356	1.280	1.431	1.291	1.364
2.000	2.000	2.000	2.000	2.000	2.000	2.000	2.000	2.000	2.000	2.000	2.000
0.042	0.073	0.068	0.063	0.066	0.048	0.060	0.076	0.051	0.060	0.081	0.099
0.424	0.384	0.289	0.307	0.363	0.338	0.472	0.322	0.360	0.285	0.355	0.318

especially from high-pressure and high-temperature regimes (e.g., Arima and Edgar, 1981) as a potential *P-T* indicator, although Ti substitutions in phlogopite are not well understood (Dymek, 1983). Various schemes have been proposed: (1) a Ti-Tschermak's end member, $2^{[4]}Si + {}^{[6]}Mg \rightleftharpoons 2^{[4]}Al + {}^{[6]}Ti$ (Robert, 1976), (2) $2^{[6]}Mg \rightleftharpoons {}^{[6]}Ti + {}^{[6]}\square$ (Bohlen et al., 1980), and (3) $^{[6]}Mg + 2(OH)^- \rightleftharpoons {}^{[6]}Ti + 2O^{2-}$ (Bohlen et al., 1980). The TiO_2 content of the SH2 phlogopites is low and ranges from 0.1 to 0.89 wt% with most values below 0.4 wt%. Figure 14 shows that the mechanism of Ti substitution does not appear to rigorously follow any of the above schemes. Nevertheless, there is a weak negative correlation with Mg. Ti is generally higher in the darker zones (Fig. 11) of zoned crystals and generally higher in deeper samples.

F in SH2 phlogopites. Although F is a minor constituent of many silicic-alkalic magma series (e.g., Bailey, 1977), recent studies (e.g., Gunow et al., 1980; Plimer, 1984) provide substantial evidence that F may have been a significant component in certain hydrothermal systems. Hydroxyl-bearing silicates, such as phlogopite, efficiently scavenge F from aqueous fluids, and F also greatly enhances the thermal stability of phlogopite (Munoz and Eugster, 1969; Foley et al., 1986). Furthermore, recent advances in curved-crystal spectrometer design allow for routine F analysis as emphasized by Petersen et al. (1982). The fluoride-hydroxyl exchange in biotite has been investigated experimentally by Munoz and Ludington (1974) in terms of the fluid composition and other intensive parameters. Hence, we analyzed for F in SH2 phlogopites in an attempt to discern any correlation with temperature, pressure, or bulk chemistry and to possibly place limits on the fluid composition. Although the geothermal solutions are Cl-bearing, the Cl content of SH2 phlogopite was usually at or below the detection limit.

The F/(F + OH) ratio for all SH2 phlogopites ranges

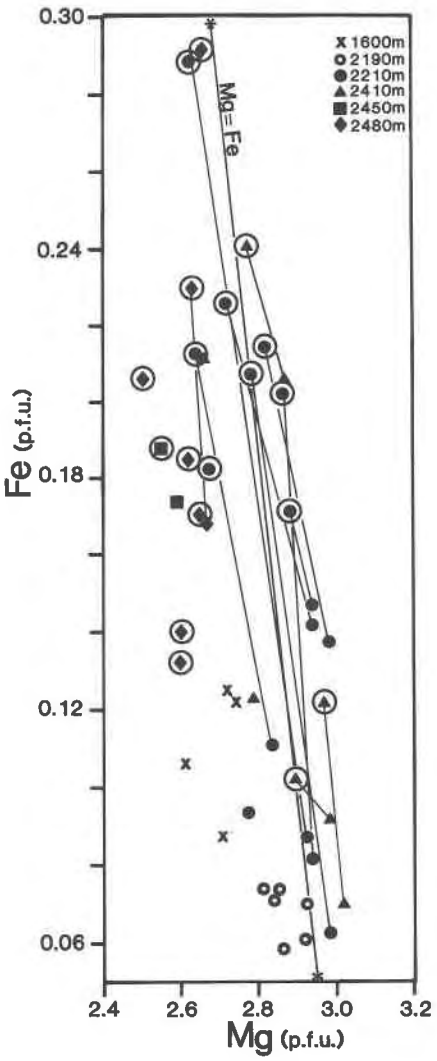

Fig. 9. The variation in SH2 phlogopites of Mg and Fe pfu on the basis of 11 oxygen equivalents. The line *—* shows the position of the substitution $Mg^{2+} \rightleftharpoons Fe^{2+}$. The circled data points indicate dark phlogopite or dark phlogopite zones. The other data points are light phlogopites or light phlogopite zones. The tielines connect dark (circled) and light zones of the same crystal. All Fe assumed to be Fe^{2+}.

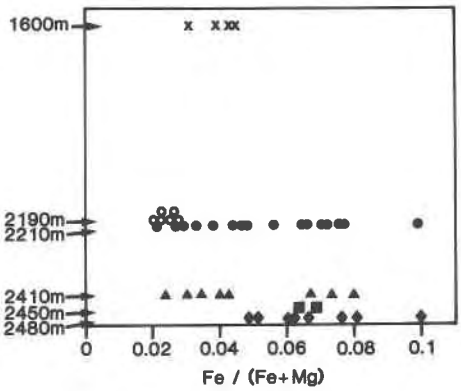

Fig. 10. Variation of Fe/(Fe + Mg) in SH2 phlogopites as a function of sample location. All Fe assumed to be Fe^{2+}.

from 0.28 to 0.57 (Table 1). Using Figure 5 of Munoz and Ludington (1974) and the temperature data derived from primary fluid inclusions in phlogopite, the $\log f_{H_2O}/f_{HF}$ values in equilibrium with the phlogopite depositing solutions are $\sim \geq 6$.

Figure 15 shows the distribution of F with respect to sample location. Although the data are limited, there is a definite maximum at 2210 m with generally lower values at greater and lesser depths.

Fe^{2+}-F avoidance. Although F substitutes freely for hydroxyl, the principle of Fe^{2+}-F avoidance—that an Fe-rich silicate requires higher f_{F_2} to stabilize a given X_F than the equivalent Mg-rich silicate—has been studied recently and emphasized by, e.g., Munoz and Ludington (1974) and Valley et al. (1982). The SH2 phlogopites have a low Fe content [Fe/(Fe + Mg) < 0.1], which may in part account for their high X_F. Figure 16 shows a positive correlation of F with Mg^{2+}. Such a good correlation is surprising considering the limited range of Mg^{2+} content and the higher uncertainty associated with F analysis.

F in phlogopite zoning. The darker zones of SH2 phlogopite (Fig. 11) generally have less F, as the Fe^{2+}-F avoidance principle would demand. However, the distribution of F in phlogopites may be more complicated. For example, although most Mg-rich (light-colored) zones have more F than do the adjacent dark zones, in three cases they had less. Furthermore, a traverse across a light-colored zone (Fig. 11) shows that the distribution is not constant.

Anhydrite trace-element chemistry

The partition coefficient of minor elements between authigenic minerals and geothermal solutions can be used to estimate some of the chemical parameters of the geothermal fluid and perhaps to resolve the precipitation mechanisms responsible for various authigenic minerals (e.g., Holland, 1956; and Shikazono et al., 1983). As a preliminary study of the trace elements in SH2 anhydrite, crystal fragments carefully handpicked from various SH2 drill-cutting samples have been analyzed by a KEVEX energy-dispersive system. Table 2 shows the data as a function of depth and gives the estimated uncertainties for Rb, Sr, Ba, La, and Ce. There are three major limitations and assumptions of this study. First, the value determined represents an average from anhydrites that perhaps were deposited by different fluids. The salinity data (Fig. 5) show that within the same sample, fluid inclusions have different values. Second, although the anhydrites were carefully examined prior to crushing, we cannot preclude the presence of contaminating phases. Third, we have assumed equilibrium crystallization between the anhydrite and precipitating solutions.

There is very little published information on the rare-

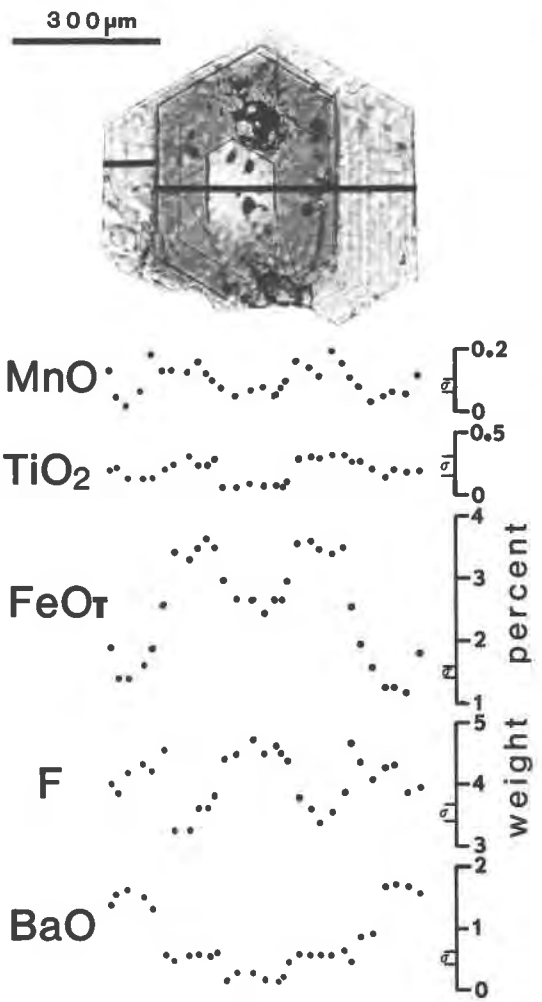

Fig. 11. An electron-microprobe traverse (offset black line) of a euhedral, zoned phlogopite crystal from the SH2 sample 2210 m. The variation of BaO, F, FeO (total Fe), TiO_2, and MnO (wt%) across the light-dark-light sequence is shown. The beam size was ~10 μm in diameter, and the standard deviation (1σ) associated with standardization is shown.

earth-element content of anhydrite; however, Morgan and Wandless (1980) presented data on two samples of hydrothermal anhydrite. Their REE values (in ppm; sample PBB-2-78, La = 91 and Ce = 180; sample PBB-3-78, La = 52 and Ce = 102) are similar to those found in the SH2 anhydrites.

The most notable and consistent aspect of the data for all elements is a minimum at 2040 m with generally increasing values to lesser and greater depths. If we compare the Ba data of anhydrite with the BaO content of coexisting phlogopite (Fig. 12), we see a similar pattern, but displaced toward slightly greater depth. Furthermore, a comparison of F in coexisting phlogopite (Fig. 15) shows a definite pattern antithetic to the anhydrite trace-element and phlogopite BaO data; the F maximum is in a similar position to their minima.

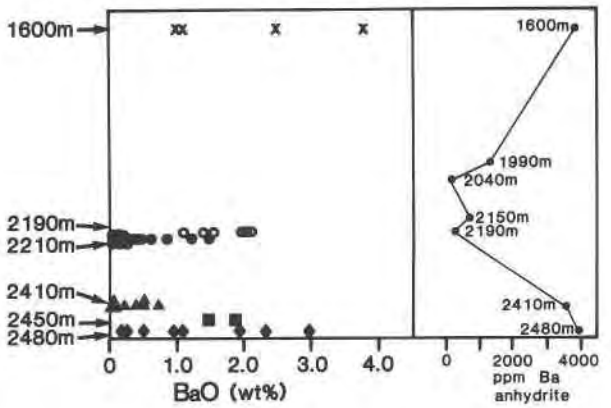

Fig. 12. The variation of BaO (wt%) of SH2 phlogopites as a function of sample location (depth in meters). The Ba (ppm) trace-element data in anhydrite are also shown.

Although the above data are limited, they corroborate our conclusions that the anhydrite and phlogopite were precipitated from the same solutions and that the factors that caused the elemental variation in both minerals were similar. The generally enriched trace-element values support the thesis that the fluid is, in part, derived from a

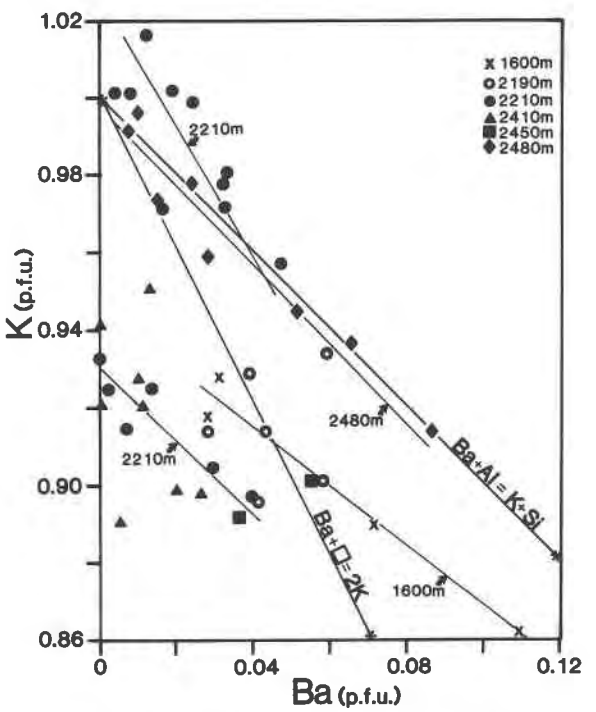

Fig. 13. The variation of K and Ba (pfu) of the SH2 phlogopites on the basis of 11 oxygen equivalents. The substitution schemes $Ba^{2+} + Al^{3+} \rightleftharpoons K^{+} + Si^{4+}$ and $Ba^{2+} + \square \rightleftharpoons 2K^{+}$ are shown as the lines *—*. Regression curves for the data from samples from 1600, 2210, and 2489 m are shown. The data for 2210 m have been divided into two groups; thus two regression curves are shown for 2210 m. 2210 m (upper curve), $r = -0.818$; 2210 m (lower curve), $r = -0.919$; 2480 m, $r = -0.970$; 1600 m, $r = -0.989$.

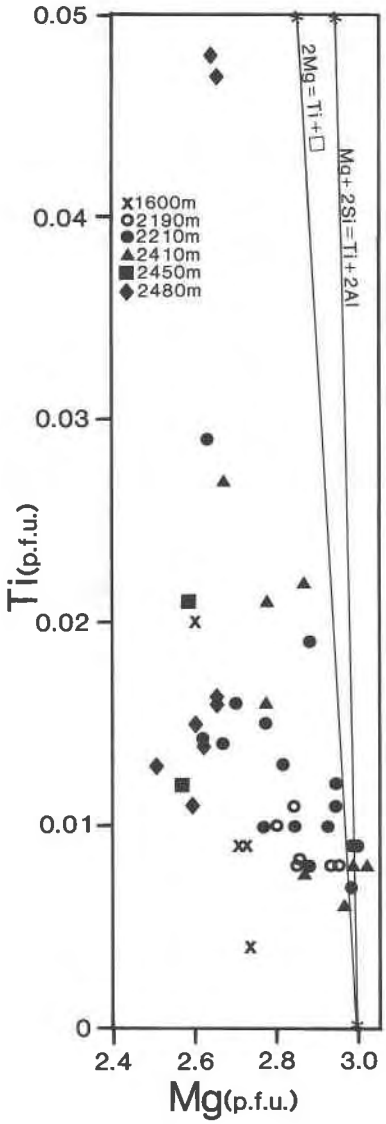

Fig. 14. The variation in SH2 phlogopites of Ti and Mg (pfu) on the basis of 11 oxygen equivalents. The substitution schemes $2Mg^{2+} \rightleftharpoons Ti^{4+} + \square$ and $Mg^{2+} + 2Si^{4+} \rightleftharpoons Ti^{4+} + 2Al^{3+}$ are shown by the lines *—*.

high-level fractionating magma (Cavarretta and Tecce, 1987).

Sr in SH2 anhydrite

Natural anhydrite contains minor amounts of Sr, which substitutes for Ca in the anhydrite structure (Purkayastha and Chatterjee, 1966). The coprecipitation of Sr with calcium sulfate minerals has been studied to try to clarify the depositional environments and especially the brine composition (e.g., Herrmann, 1961; Butler, 1973; Kushnir, 1982a). However, experimental studies of the partitioning of Sr between anhydrite and aqueous solutions at

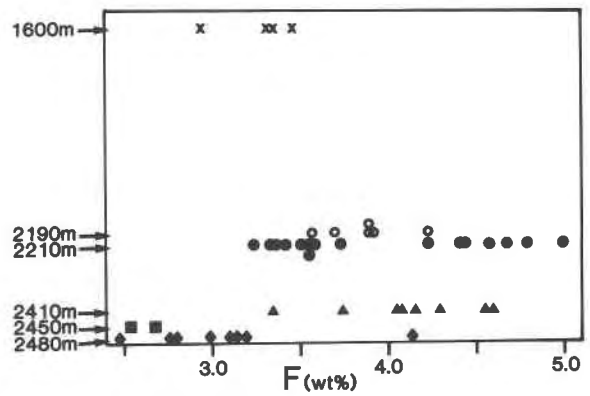

Fig. 15. The variation of F (wt%) in SH2 phlogopites as a function of sample location (depth in meters).

various salinities, pressures, and temperatures are limited (e.g., Kushnir, 1982b; Shikazono and Holland, 1983).

The distribution of Sr and Ca between two phases is governed by the equation

$$K_{BN} = (a_{SrSO_4}/a_{CaSO_4})/(a_{Sr^{2+}}/a_{Ca^{2+}}),$$

where K_{BN} is the distribution coefficient, a_{SrSO_4} and a_{CaSO_4} are the activities of the $SrSO_4$ and $CaSO_4$ components of anhydrite, and $a_{Sr^{2+}}$ and $a_{Ca^{2+}}$ are the activities of Sr^{2+} and Ca^{2+} in solution. K_{BN} is a Berthelot-Nernst–type distribution coefficient (e.g., McIntire, 1963).

We have calculated the Sr/Ca ratio in the precipitating brine for four samples (Table 3). Kushnir (1982a) studied the partitioning of Sr between anhydrite and brine during gypsum to anhydrite transformation at temperatures below 150 °C. He found a linear decrease of K_d^{Sr} with temperature. Shikazono and Holland (1983) found that K_d^{Sr} depends less on the NaCl concentration, temperature, and precipitation rate than on the degree of supersaturation of the solutions with respect to anhydrite and/or the morphology of the precipitated anhydrite crystals. They distinguished acicular and rectangular anhydrite. The rectangular anhydrite morphology is similar to the SH2 anhydrite. The Shikazono and Holland (1983) K_d^{Sr} values between solution and rectangular anhydrite at 150, 200, and 250 °C are 0.35, 0.24, 0.27 (±0.05), respectively. Note that they show a minimum at 200 °C. Thus, using these experimental K_d^{Sr} values, the Sr/Ca ratio in the precipitating solution ranges from 0.060 to 0.10. However, the experimental K_d^{Sr} values do not agree with the higher K_d^{Sr} values of natural hydrothermal anhydrites from the East Pacific Rise (Shikazono and Holland, 1983) or from vein anhydrites from the Salton Sea geothermal system (M. A. McKibben, pers. comm., 1987). The Sr/Ca ratio of sea water (~0.021) is significantly different from those values (Table 3) calculated with the experimental K_d^{Sr} data. If the higher, natural K_d^{Sr} values are used, the SH2 Sr/Ca ratio would be closer to the sea-water ratio. Thus, we cannot preclude the presence of sea water as a component in the SH2 geothermal fluid.

TABLE 2. XRF-KEVEX analyses (in ppm) of anhydrite separates from ther SH2 well

	Depth of drillcutting sample (m)							
	1300	1600	1990	2040	2150	2190	2410	2480
Rb	190	320	100	40	110	130	450	670
Sr	6100	5700	6200	2000	5100	8400	5600	5400
Ba	1600	3800	1300	110	730	280	3600	3900
La	400	70	30	<2	14	50	110	130
Ce	500	80	20	16	50	30	210	180

Note: John R. Evans, analyst. The uncertainty is ±5% of the given value except for values <20, where the uncertainty is ±10%.

DISCUSSION

Deposition of anhydrite

Quartz, calcite, and anhydrite are perhaps the three most common primary gangue minerals in hydrothermal ore deposits (Samartsev et al., 1980; Shikazono et al., 1983; Drummond and Ohmoto, 1985). The conditions that deposit anhydrite are of interest to help model the geothermal and ore-forming environments. Geothermal solutions at the SH2 well site have deposited anhydrite as the result of perhaps various processes.

Anhydrite solubility in pure water at geothermal temperatures is retrograde; however, the retrograde solubility reaches a minimum with increasing NaCl content at constant pressure (Blount and Dickson, 1969). Blount and Dickson (1969) also found that a pressure increase raises the solubility of anhydrite over the entire range of their experimental conditions. However, the retrograde effect of increasing temperature far outweighs the positive effect of increasing pressure except in NaCl solutions greater than 2*M*. The range of salinity from our fluid-inclusion studies in SH2 anhydrite is 0.5 to 14.0 wt% NaCl equivalent, which corresponds to ~0 to ~2*M* NaCl. Thus, the effect of a minimum in anhydrite solubility as a function of salinity would be minimized in SH2 solutions. However, the presence of the other dissolved components (Ba^{2+}, Sr^{2+}) and volatiles (CO_2, B, HF, hydrocarbons) may have significantly enhanced this minimum solubility effect.

Drummond and Ohmoto (1985) have modeled boiling hydrothermal systems and concluded that anhydrite, and sulfates in general, will not be common depositional products of boiling. However, in relatively dilute and slightly acidic solutions of about 250 °C, the decrease in proton concentration associated with boiling can cause sulfate minerals (anhydrite) to precipitate (Sasada, 1986). Queen and Motyka (1984) found that in water-dominated zones of the Makushin geothermal system, anhydrite is a common authigenic mineral, whereas it is absent from the vapor-dominated zones. We find no petrographic evidence for boiling in SH2, and the measured down-hole temperatures and the similar homogenization temperatures lie far to the left of the depth with boiling-point curve calculated for this environment.

Shikazono et al. (1983) have examined the mode of anhydrite occurrence and its depositional mechanisms in Kuroko deposits. Fluid inclusions in these Kuroko anhydrites have T_h values that range from 240 to 340 °C with salinity values from 0 to 5 wt% NaCl equivalent. They concluded on the basis of these data, Sr concentrations, and $^{87}Sr/^{86}Sr$ ratios that anhydrite deposition was the result of a subsurface mixing of fluids. Although we find some evidence for perhaps multiple fluids at SH2, our data are insufficient to discuss deposition by this mechanism conclusively.

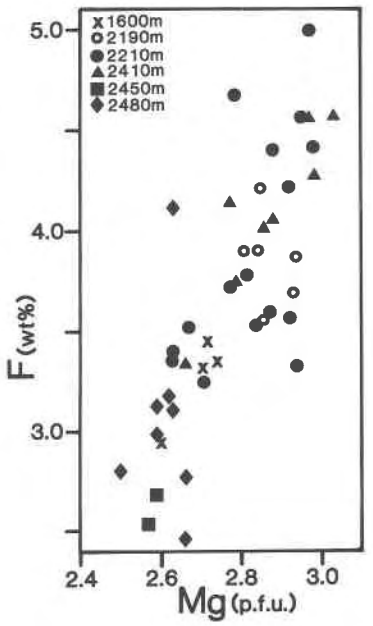

Fig. 16. The variation of Mg (pfu) (on the basis of 11 oxygen equivalents) and F (wt%) in SH2 phlogopites.

Phlogopite and biotite in geothermal systems

Biotite is a common primary constituent of the host rock in many geothermal systems but is rare as a hydrothermal mineral (Browne, 1984) except in the deeper, higher-temperature portions of some geothermal systems. Biotite appears between the 325 and 360 °C interval in Borehole Elmore 1, Salton Sea geothermal field (McDowell and Elders, 1980), in the hotter (>325 °C) parts of the Cerro Prieto field (Elders et al., 1979), at Ngawha, New Zealand, at temperatures above 220 °C (Browne, 1984), and in wells MF2, MF5, and SV3 in the Phlegraean

TABLE 3. Calculation of the Sr/Ca ratio in the geothermal fluid of the SH2 well

Sample depth (m)	In-hole *T* (°C)	Sr ppm (Table 2)	K_d^{Sr*}	Calculated fluid Sr/Ca
1300	143	6100	0.35	0.060
1600	190	5700	0.24	0.082
2150	~250	5100	0.27	0.064
2190	~250	8400	0.27	0.10

* Shikazono and Holland (1983).

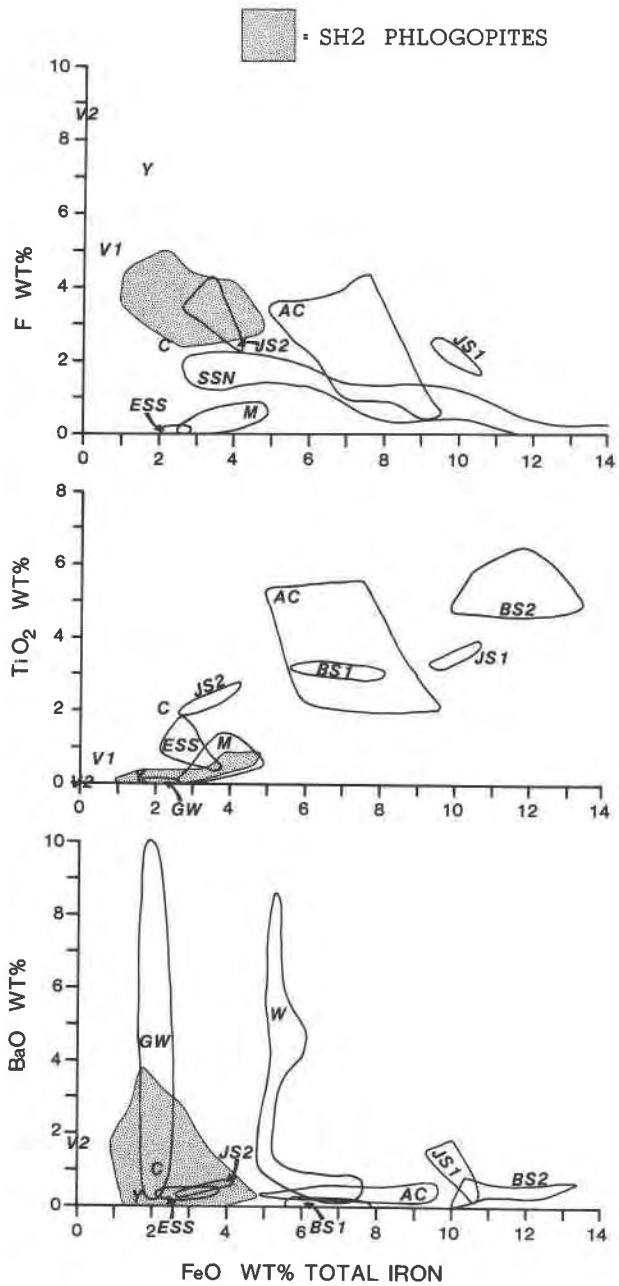

Fig. 17. A comparison of the F, TiO_2, and BaO vs. FeO variations for SH2 and other phlogopites. ESS = Exley et al. (1982), host = spinel lherzolite (F was not detected in micas with FeO > 3 wt%). M = Matson et al. (1986), host = peridotite xenoliths (primary and secondary) and mica-rich xenoliths (glimmerite) in kimberlite. BS1, BS2 = Bachinski and Simpson (1984), host = minettes, BS1 = group I phenocrysts, BS2 = group II groundmass. JS1, JS2 = Jones and Smith (1985), host = minettes, JS1 = Hannaborough Quarry locality, JS2 = Loxbeare Farm locality. V1, V2 = Valley et al. (1982), host = marble, V1 = sample GOV50-2, V2 = sample BMT-1 (BaO for GOV50-2 was not determined). W = Wendlandt (1977), host = monticellite peridotite. GW = Gaspar and Wyllie (1982), host = carbonatites. Y = Yau et al. (1984), host = granulite-facies (metasedimentary) retrograde calcsilicate rock. SSN = Schulze et al. (1985), host = lamprophyres. C = Cross (1897), host = wyomingite. AC = Allan and Carmichael (1984), host = lamprophyric lavas.

Fields at temperatures above 300 °C (Belkin et al., 1986). Cavarretta et al. (1985) reported biotite as a contact metasomatic mineral at or above 300 °C in the Latera geothermal field, Italy. Biotite is also reported in the SH2 well as an uncommon phase below 1600 m and above 200 °C (Cavarretta and Tecce, 1987). Another phyllosilicate not generally found in geothermal systems is lepidolite. However, from Yellowstone National Park boreholes, Bargar et al. (1973) reported lepidolite forming between 130 and 140 °C. Phlogopite is also a rare authigenic mineral in geothermal fields. Cavarretta et al. (1985) reported phlogopite from the Latera geothermal field, Italy, in the contact metasomatic zone above 200 °C. Phlogopite has also been reported in paleohydrothermal systems. Zhang (1986) reported the assemblage phlogopite + anhydrite (with pyrite) from a volcanic area in the Yangtze River valley. Fluid-inclusion studies in the anhydrite indicate the temperature to be between 300 and 500 °C.

The common occurrence of authigenic phlogopite in the SH2 well indicates that equilibrium crystallization of phlogopite can occur at temperatures from ~200 to ~300 °C and pressures from 140 to 220 bars from a F-bearing, volatile-rich, generally dilute geothermal solution.

Comparison with phlogopites from other environments

Phlogopite is often the only volatile-bearing constituent of mantle-derived rocks and potassic mafic and ultramafic rocks. Because of its petrogenetic importance, geothermometers and geobarometers involving various elemental variations have been proposed (e.g., Luhr et al., 1984; Tronnes et al., 1985). Figure 17 shows a comparison of F, TiO_2, and BaO vs. FeO as total Fe between the SH2 phlogopites and phlogopites or phlogopitic biotites from different metamorphic and igneous environments. This is not a comprehensive survey and was further limited by the paucity of studies that provided data on all three elements—F, Ba, and Ti. Minor-element abundances in any mineral are a complex interrelationship of intensive and extensive parameters. SH2 phlogopites represent compositions formed from a low-temperature, low-pressure, aqueous, volatile-rich environment and might be used to constrain the lower-pressure, lower-temperature stability field of phlogopite compositions.

A generally negative correlation of F with FeO is apparent (Fig. 17) and would be consistent with the crystal-chemical rule of Fe^{2+}-F avoidance. Two fields of phlogopites (M, ESS, Fig. 17) from kimberlites and spinel lherzolites have a low F content with respect to other phlogopites with similar FeO content and probably represent the influence of a low-F bulk composition. A positive correlation of TiO_2 with FeO (Fig. 17) suggests that, in general, the substitution $Mg^{2+} \rightleftharpoons Fe^{2+}$ controls the Ti content and/or a bulk composition richer in Fe is also

richer in Ti. The position of the F and Ti SH2 phlogopite compositional fields with respect to other fields suggests that neither pressure nor temperature alone control Ti or F variation.

The pattern of BaO distribution (Fig. 17), however, suggests that the major controlling factor in the Ba content of phlogopites is the bulk composition. In general, phlogopite has BaO values of 1 wt% or less. Three fields (SH2 phlogopites, GW, W) are major exceptions. The replacement of K^+ by Ba^{2+} in the phlogopite interlayer site requires charge compensation that can be achieved by various substitution schemes (see above). Higuchi and Nagasawa (1969) and Jensen (1973) reported partition coefficients in a dacite—K_{Ba} for biotite/matrix of ~10 and K_K for biotite/matrix of ~2. Thus, phlogopite would act as a very effective scavenger of Ba. The variability of BaO at relatively constant FeO content in the SH2 phlogopites suggests significant Ba variations in the geothermal fluid.

Hydrocarbons in the inclusion fluid

The occurrence of liquid hydrocarbons and a gas-clathrate with a melting temperature significantly greater than 10 °C are not common in the fluid inclusions in the SH2 anhydrites. The presence of hydrocarbons in geothermal and hydrothermal environments is not unusual (e.g., Roedder, 1984; Hodge and Norman, 1985), especially if such environments are located in, or if the fluid passed through, a sedimentary sequence. Thus, the presence of hydrocarbons in the SH2 inclusion fluid suggests some interaction with or fluid derivation from the local sedimentary environment.

CO_2 in the inclusion fluid

The evidence for CO_2 as a volatile constituent in fluid inclusions in SH2 anhydrite is widespread but not universal. Crushing and freezing data suggest that during some anhydrite-depositional periods, the percipitating fluid contained CO_2. Because the drill-cutting sample may represent the entire depositional time range, each sample would tend to show the complete range of fluid compositions. The minimum CO_2 concentration necessary to produce CO_2 clathrate in liquid-rich inclusions trapped in the temperature range of 200 to 300 °C is 1.5 mol% (Sasada, 1985).

The rare occurrence of liquid-CO_2 fluid inclusions from geothermal fields has been discussed by Sasada (1985). He has argued that pressures greater than hydrostatic are necessary to form inclusions with liquid CO_2 (at room temperature) in the geothermal environment. A vein system, sealed by mineral deposition, could represent such a circumstance. The self-sealed vein system could still be subject to greater than lithostatic pressure from the ascending fluid, especially if some or all of the ascending liquids and volatiles evolved from crystallizing magma. In the SH2 well, the abundant filled and cross-cutting veins suggest that such overpressure resulted in common hydrofracturing, subsequent self-sealing of fracture permeability by mineral deposition, and then repeated hydrofracturing.

Evolution of the geothermal system

A comparison of the well-fluid composition and meaured in-hole temperatures with the fluid inclusion T_h and salinity data would allow an assessment of geothermal evolution (e.g., Browne et al., 1976; Belkin et al., 1986). However, because no fluid was recovered from the SH2 well, our analysis is limited.

The correspondence of the T_t data (Fig. 4) for anhydrite with in-hole temperatures is quite good. The scatter of the T_t values and especially the low T_t values from 2410 m could result from one or a combination of factors: (1) the hydrologic regime (water table) was different at the time of trapping than the regime that exists today, and hence the pressure correction is in error; (2) the drill-cutting samples may have significant vertical—and hence temperature—scatter; (3) inclusions that had necked-down were measured; and (4) the sample may represent several different times, temperatures, or pressures of formation. The T_t data (Fig. 6) of phlogopite show a similar correspondence to the in-hole temperature. The data are less numerous than the T_t data for anhydrite, and this undoubtedly adds to the scatter. Nevertheless, the T_t data for anhydrite and phlogopite indicate that these authigenic phases are relatively recent and/or the thermal flux of the water-dominated geothermal system has remained stable during the latter stages of its evolution. The salinity data for anhydrite and phlogopite (Figs. 4 and 5) suggest the existence of multiple fluids that resulted in the trapping of a range of salinities (~0 to ~14 wt% NaCl equivalent). However, the data are too limited to define any systematics between sample location and host.

An episodic and multiple-fluid environment

The large-scale (light-dark, etc.) zoning in some SH2 phlogopites and their element variations indicate an episodic and/or multiple-fluid environment during the evolution of the SH2 geothermal system. The major phlogopite color-zone difference is associated with the Mg-Fe substitution. The dark zones are enriched in Fe but depleted in F relative to the light zones. A plausible explanation for such a distribution would be the episodic introduction of magmatic fluid into the geothermal regime. A fluid, perhaps derived from a fractionating trachytic magma (Cavarretta and Tecce, 1987), would be enriched in HF and other volatile species (CO_2, etc.). This would reduce the activity of H_2O and hence the activity of Fe. Phlogopite crystallizing at this time would be depleted in Fe but enriched in F. The common sharp, color-zone boundaries suggest that these pulses produced relatively rapid changes in fluid conditions. Cavarretta and Tecce (1987) have reported similar zoning in vesuvianite and suggested that it has resulted from the process of episodic hydrofracturing. Uncommon phlogopite dissolution textures also suggest that during some periods the fluid became undersaturated with respect to phlogopite.

The BaO distribution in the phlogopites, where, for example, light zones can be enriched or depleted with respect to the dark zones, suggests that the episodic conditions are not just the simple alternation of two uniform fluid compositions or physicochemical conditions. The Ba distribution indicates that each fluid pulse was somewhat different with respect to some components. This argues for an evolving magmatic fluid or varying degrees of interaction (mixing) with another Ba-rich fluid. It is interesting to note that the first Ba-rich igneous biotite, containing 7.32 wt% BaO, was reported by Thompson (1977) from a leucitite from the Alban Hills, Italy, a similar volcanic district in the perpotassic Roman province. Subsequent reported Ba-rich biotites from similar feldspathoid-bearing volcanic rocks are interpreted as late-crystallizing phases.

Although the element distribution can be zoned within a single phlogopite crystal, the element distribution with respect to sample location (depth) in the phlogopites and anhydrites also indicates zoning. The stratigraphic interval from approximately 2000 to 2200 m shows a general depletion of BaO in phlogopite and trace elements in anhydrite and an enrichment of F in phlogopite. This suggests a stratigraphic zone where the presence of a fluid rich in Ba, Sr, and other trace elements was limited. This implies lithologic and/or permeability differences or perhaps a fluid stratification (Oakes, 1985).

The origin and evolution of various S species in geothermal systems related to volcanic districts is the subject of continual investigation and debate (e.g., Kiyosu and Kurahashi, 1983). Furthermore, the presence of SO_2 and stable igneous sulfate minerals (e.g., anhydrite) in magmas and their products has received considerable renewed interest, especially after the eruption of El Chichón in 1982 (Luhr et al., 1984). Rye et al. (1984) argued on the basis of stable isotopes that a major source of the high El Chichón S content (pre-eruption, ~2.6 wt% SO_3) must be, in part, magmatic and thus the S was not entirely remobilized from nearby evaporites. The release of SO_2 as part of the volatile magma fraction degassing from the upper portions of a fractionating magma will eventually allow the S to become part of a hot ascending aqueous fluid. These S and other volcanic exhalations will participate in reactions with magmatic, connate, and/or meteoric aqueous fluids. Kiyosu and Kurahashi (1983) suggested that the sulfate-rich waters in volcanic areas result from a disproportionation reaction of SO_2 to yield the more oxidized sulfate species. H_2S is also produced and would tend to react with available Fe to form, for example, pyrite—a ubiquitous accessory in the SH2 well. Thus, it is reasonable to assume that the S present in the SH2 well could be partially magmatic and that appeal to the remobilization of Mesozoic evaporites as the sole S source is unnecessary. Bertrami et al. (1986) compared the $\delta^{18}O$ and $\delta^{13}C$ in calcites from various Latium geothermal wells and their host Mesozoic carbonates. The $\delta^{18}O$ of SH2 calcites is significantly different from the Mesozoic carbonates, being more than 20‰ lighter. This suggests a possible magmatic source for the geothermal CO_2. Cortecci et al. (1980) reported that the $\delta^{34}S$ values for sulfate from the Cesano C-1 well brine and anhydrites from the Cesano RC-1 well show similar values of about +15‰, but quite different $\delta^{18}O$ values of +4.8‰ and +14.9‰ ± 0.3‰, respectively. The low $\delta^{18}O$ value of +4.8‰ suggests that the origin of the Cesano sulfates may not be just the simple dissolution and reprecipitation of Upper Triassic sedimentary evaporites.

A detailed S- and Sr-isotope study of the authigenic mineral assemblage in the SH2 well would provide valuable information on the origin and evolution of the SH2 geothermal fluid.

Conclusions

1. Phlogopite and anhydrite (plus pyrite and calcite) occur as authigenic and hydrothermal minerals in fracture and pore-space fillings in the SH2 geothermal well, located in the Sabatini volcanic district, Latium, Italy. Also present in the well, at various levels, are K-feldspar, garnet, vesuvianite, apatite, spinel, pyroxene, wollastonite, wilkeite, cuspidine, harkerite, cancrinite, and reyerite.

2. The primary fluid inclusions in phlogopite and the primary and secondary fluid inclusions in anhydrite have vapor-liquid homogenization temperatures similar to the measured in-hole temperature of the SH2 well. This indicates that the minerals are relatively recent and/or that the thermal regime has remained stable during the past. The salinity data show a considerable scatter; this and the rare occurrence of hydrocarbons and daughter crystals indicate the presence of fluids with different compositions. Crushing data, clathrate formation, and the rare occurrence of liquid CO_2 also indicate that CO_2 was a common volatile species.

3. Detailed microprobe analyses of unzoned and zoned phlogopite crystals that contain primary fluid inclusions reveal that they have nearly end-member compositions, with Fe/(Fe + Mg) = 0.02 to 0.1, and have variable contents of F, BaO, and TiO_2. This variability is directly related to the phlogopite zoning and sample location. The crystal zoning indicates episodic changes in growth conditions whereas the variation with depth also suggests some kind of lithologic (permeability?) control on growth conditions, e.g., fluid mixing.

4. Energy-dispersive trace-element analysis of anhydrite crystals shows a relatively high abundance of Sr, Ba, Rb, Ce, and La. The overall variation of anhydrite composition with sample location is similar to that of the variation of phlogopite chemistry with sample location and suggests a similar and related control in growth conditions.

5. The fluid-inclusion salinity data, the presence of zoned phlogopites, and the compositional variation among different samples of phlogopite and anhydrite reveal a picture of episodic and/or changing fluid and/or mineral growth conditions during the evolution of the SH2 geothermal field. The presence of hot, mineral-rich, ascending solutions has effectively reduced the permeability of the host

rock by successive episodes of deposition in pore spaces and fractures.

Acknowledgments

The AGIP-ENEL Joint Venture is gratefully acknowledged for supplying the samples and drilling data of the SH2 well. Dr. Jean Dubessy of CREGU (Nancy, France) kindly allowed access and instruction (F. T.) for the laser Raman probe. Financial support to this project for G. C., B. D. V., and F. T. was provided by C.N.R., Gruppo Nazionale di Vulcanologia. We thank Malcom Ross (USGS) for determining the phlogopite crystallography and John R. Evans (USGS) for the KEVEX analyses. We also thank Elaine S. McGee (USGS) and Marta J. K. Flohr (USGS) for stimulating discussions concerning phlogopite chemistry. The manuscript benefited from the careful reviews of E. Roedder, M.J.K. Flohr, and M. A. McKibben.

References cited

Allan, J.F., and Carmichael, I.S.E. (1984) Lamprophyric lavas in the Colima graben, SW Mexico. Contributions to Mineralogy and Petrology, 88, 203–216.

Arima, M., and Edgar, A.D. (1981) Substitution mechanisms and solubility of titanium in phlogopites from rocks of probable mantle origin. Contributions to Mineralogy and Petrology, 77, 288–295.

Bachinski, S.W., and Simpson, E.L. (1984) Ti-phlogopites of the Shaw's Cove minette: A comparison with micas of other lamprophyres, potassic rocks, kimberlites, and mantle xenoliths. American Mineralogist, 69, 41–56.

Bailey, J.C. (1977) Fluorine in granitic rocks and melts, a review. Chemical Geology, 19, 1–42.

Baldi, P., Decandia, F.A., Lazzarotto, A., and Calamai, A. (1974) Studio geologico del substrato della copertura vulcanica laziale nella zona dei laghi di Bolsena, Vico e Bracciano. Memorie della Società Geologica Italiana, 13, 575–606.

Bargar, K.E., Beeson, M.H., Fournier, R.O., and Muffler, L.J.P. (1973) Present-day deposition of lepidolite from thermal waters in Yellowstone National Park. American Mineralogist, 58, 901–904.

Baronnet, A., and Velde, B. (1977) Iron content of synthetic phlogopite as a function of growth rate. Earth and Planetary Science Letters, 37, 150–153.

Belkin, H.E., De Vivo, B., Roedder, E., and Cortini, M. (1985) Fluid inclusion geobarometry from ejected Mt. Somma-Vesuvius nodules. American Mineralogist, 70, 288–303.

Belkin, H.E., Chelini, W., De Vivo, B., and Lattanzi, P. (1986) Fluid inclusions in hydrothermal minerals from Mofete 2, Mofete 5 and San Vito 3 geothermal wells, Phlegrean Fields, Campania, Italy. International Volcanological Congress, Proceedings of Symposium 5: Volcanism, Hydrothermal Systems and Related Mineralization, 7–12.

Bertrami, R., Friedman, I., Gleason, J., Lombardi, S., and Pandeli, E. (1986) Isotopic composition of carbon and oxygen in the carbonate materials present in Italian geothermal wells: On their genesis and geothermometric application. Fifth International Symposium on Water-Rock Interaction, Iceland, Extended Abstracts, 56–59.

Blount, C.W., and Dickson, F.W. (1969) The solubility of anhydrite ($CaSO_4$) in NaCl-H_2O from 100 to 450 °C and 1 to 1000 bars. Geochimica et Cosmochimica Acta, 33, 227–245.

Bohlen, S.R., Peacor, D.R., and Essene, E.J. (1980) Crystal chemistry of metamorphic biotite and its significance in water barometry. American Mineralogist, 65, 55–62.

Browne, P.R.L. (1984) Lectures on geothermal geology and petrology. The United Nations University, Geothermal Training Programme, Iceland, Report 1984-2, 92 p.

Browne, P.R.L., Roedder, E., and Wodzicki, A. (1976) Comparison of past and present geothermal waters, from a study of fluid inclusions, Broadlands field, New Zealand. In J. Cadek, and T. Paces, Eds., Proceedings, International symposium on water-rock interaction, Czechoslovakia, 1974, Geological Survey, Prague, 140–149.

Butler, G.P. (1973) Strontium geochemistry of modern and ancient calcium sulphate minerals. In B.H. Purser, Ed., The Persian Gulf, p. 423–452. Springer, Berlin.

Calamai, A., Cataldi, R., Dall'Aglio, M., and Ferrara, G.C. (1975) Preliminary report on the Cesano hot brine deposit (Northern Latium, Italy). United Nations Symposium of Geothermal Energy, San Francisco, California, 1, 305–313.

Calamai, A., Fiordelisi, A., Pandeli, E., and Valenti, P. (1985) First exploratory well in the Sabatini area (northern Latium). In A.S. Strub and P. Ungemach, Eds., European geothermal update, p. 433–439. Proceedings of the Third International Seminar on the Results of EC Geothermal Energy Research, Munich, 1983.

Cavarretta, G., and Tecce, F. (1987) Contact metasomatic and hydrothermal minerals in the SH2 deep well, Sabatini volcanic district, Latium, Italy, Geothermics, 16, 127–145.

Cavarretta, G., Gianelli, G., and Puxeddu, M. (1982) Formation of authigenic minerals and their use as indicators of the physicochemical parameters of the fluid in the Larderello-Travale geothermal field. Economic Geology, 77, 1071–1084.

Cavarretta, G., Gianelli, G., Scandiffio, G., and Tecce, F. (1985) Evolution of the Latera geothermal system II: Metamorphic, hydrothermal mineral assemblages and fluid chemistry. Journal of Volcanology and Geothermal Research, 26, 337–364.

Collins, P.L.F. (1979) Gas hydrates in CO_2-bearing fluid inclusions and the use of freezing data for estimation of salinity. Economic Geology, 74, 1435–1444.

Cortecci, G., Bertrami, R., and Ceccarelli, A. (1980) Circulation patterns and geothermometry of some Italian spring systems by sulfate isotopes. Third International Symposium on Water-Rock Interaction, Edmonton, Extended Abstracts, 115–116.

Crawford, M.L. (1981) Phase equilibria in aqueous fluid inclusions. In L.S. Hollister and M.L. Crawford, Eds., Fluid inclusions: Applications to petrology, p. 75–100. Mineralogical Association of Canada Short Course Handbook.

Cross, W. (1897) Igneous rocks of the Leucite Hills and Pilot Butte, Wyoming. American Journal of Science, fourth series, 4, 115–141.

Cundari, A. (1979) Petrogenesis of leucite-bearing lavas in the Roman volcanic region, Italy: The Sabatini lavas. Contributions to Mineralogy and Petrology, 70, 9–21.

De Rita, D., Funiciello, R., Rossi, U., and Sposato, A. (1983) Structure and evolution of the Sacrofano-Baccano caldera, Sabatini volcanic complex, Rome. Journal of Volcanology and Geothermal Research, 17, 219–236.

Dhamelincourt, P., Beny, J.M., Dubessy, J., and Poty, B. (1979) Analyses d'inclusions fluides à la microsonde MOLE à effet Raman. Bulletin de Minéralogie, 102, 600–610.

Di Filippo, M., Funiciello, R., and Parotto, M., Eds. (1984) Geological map of the Sabatini area. Conisiglio Nazionale delle Ricerche Progetto Finalizzato Geodinamica.

Di Girolamo, P. (1978) Geotectonic setting of Miocene-Quaternary volcanism in and around eastern Tyrrhenian Sea border (Italy) as deduced by major element geochemistry. Bulletin Volcanologique, 42–43, 229–250.

Drummond, S. E., and Ohmoto, H. (1985) Chemical evolution and mineral deposition in boiling hydrothermal systems. Economic Geology, 80, 126–147.

Dymek, R. F. (1983) Titanium, aluminum and interlayer cation substitutions in biotite from high-grade gneisses, West Greenland. American Mineralogist, 68, 880–899.

Elders, W.A., Hoagland, J.R., McDowell, S.D., and Cobo R., J.M. (1979) Hydrothermal mineral zones in the geothermal reservoir of Cerro Prieto. In W.A. Elders, Ed., Geology and geothermics of the Salton Trough, Field Trip no. 7, p. 36–43. Geological Society of America 92nd Annual Meeting, November 1979.

Exley, R. A., Sills, J. D., and Smith, J. V. (1982) Geochemistry of micas from the Finero spinel-lherzolite, Italian Alps. Contributions to Mineralogy and Petrology, 81, 59–63.

Fisher, J.R. (1976) The volumetric properties of H_2O—A graphical portrayal. U.S. Geological Survey Journal of Research, 4, 189–193.

Flohr, M.J.K. (1983) BASIC programs for calculation of cation site occupancies and plotting of mineral data with applications for evaluation of metamorphic mineral assemblages. U.S. Geological Survey, Open-File Report 83-905, 65 p.

Foley, S.F., Taylor, W.R., and Green, D.H. (1986) The effect of fluorine

on phase relationships in the system $KAlSiO_4$-$MgSiO_4$-SiO_2 at 28 kbar and the solution mechanism of fluorine in silicate melts. Contributions to Mineralogy and Petrology, 93, 46–55.

Funiciello, R., and Parotto, M. (1978) Il substrato sedimentario nell' area dei Colli Albani: Considerazioni geodinamiche e paleogeografiche del margine tirrenico dell'Appennino centrale. Geologica Romana, 17, 233–287.

Gaspar, J.C., and Wyllie, P.J. (1982) Barium phlogopite from the Jacupiranga carbonatite, Brazil. American Mineralogist, 67, 997–1000.

Gunow, A.J., Ludington, S., and Munoz, J.L. (1980) Fluorine in mica from the Henderson molybdenite deposit, Colorado. Economic Geology, 75, 1127–1137.

Haas, J.L., Jr., (1971) The effect of salinity on the maximum thermal gradient of a hydrothermal system at hydrostatic pressure. Economic Geology, 66, 940–946.

Hattori, K., Cameron, E.M., and Smith, R. (1985) Occurrence and geochemistry of anhydrite in the Hemlo Basin. Geological Association of Canada and Mineralogical Association of Canada, Joint Annual Meeting 1985, Program with Abstracts, 10, A25.

Hedenquist, J.W., and Henley, R.W. (1985) Effect of CO_2 on freezing point depression measurements of fluid inclusions—Evidence from active systems and implications for epithermal ore deposition. Economic Geology, 80, 1379–1406.

Herrmann, A.G. (1961) Zur Geochimie des Strontiums in den salinaren Zechstein abbgerunngun der Stassfurt serie die Subharzbezirkes. Chemie der Erde, 21, 137–194.

Higuchi, H., and Nagasawa, H. (1969) Partition of trace elements between rock-forming minerals and the host volcanic rocks. Earth and Planetary Science Letters, 7, 281–287.

Hodge, G., and Norman, D.I. (1985) Organic compounds in epithermal ore-depositing fluids (abs). In Epithermal Deposits in New Mexico. New Mexico Bureau of Mines and Mineral Resources Circular 199, 53.

Holland, H.D. (1956) The chemical composition of vein minerals and the nature of ore forming fluids. Economic Geology, 51, 781–797.

Jensen, B.B. (1973) Patterns of trace element partitioning. Geochimica et Cosmochimica Acta, 37, 2227–2242.

Jones, A.P., and Smith, J.V. (1985) Phlogopite and associated minerals from Permian minettes in Devon, South England. Bulletin of the Geological Society of Finland, 57, part 1–2, 89–102.

Keenan, J.H., Keyes, F.G., Hill, P.G., and Moore, J.G. (1969) Steam tables: Thermodynamic properties of water including vapor, liquid and solid phases, 162 p. Wiley, New York.

Kiyosu, Y., and Kurahashi, M. (1983) Origin of sulfur species in acid sulfate-chloride thermal waters, northeastern Japan. Geochimica et Cosmochimica Acta, 47, 1237–1245.

Kozlova, O.G., Stepanova, T.V., and Egorov-Tismenko, Yu.K. (1984) The mica law of twinning and the formation of primary inclusions. Vestnik Moskovskogo Universiteta. Geologiya, 39, no. 3, 52–57 (translated in Moscow University Geology Bulletin, 1984, 39, no. 3, 54–60).

Kushnir, J. (1982a) The partitioning of seawater cations during the transformation of gypsum to anhydrite. Geochimica et Cosmochimica Acta, 46, 433–446.

——— (1982b) The composition and origin of brines during the Messinian desiccation event in the Mediterranean basin as deduced from concentrations of ions coprecipitated with gypsum and anhydrite. Chemical Geology, 35, 333–350.

Luhr, J.F. Carmichael, I.S.E., and Varekamp, J.C. (1984) The 1982 eruptions of El Chichón volcano, Chiapas, Mexico: Mineralogy and petrology of the anhydrite-bearing pumices. Journal of Volcanology and Geothermal Research, 23, 69–108.

Matson, D.W., Muenow, D.W., and Garcia, M.O. (1986) Volatile contents of phlogopite micas from South African kimberlite. Contributions to Mineralogy and Petrology, 93, 399–408.

McDowell, S.D., and Elders, W.A. (1980) Authigenic layer silicate minerals in Borehole Elmore 1, Salton Sea geothermal field, California, USA. Contributions to Mineralogy and Petrology, 74, 293–310.

McGee, J.J. (1983) $ANBA, a rapid, combined data acquisition and correction program for the SEMQ electron microprobe. U.S. Geological Survey Open-File Report 83-817, 45 p.

McIntire, W.L. (1963) Trace element partition coefficients—A review of theory and application to geology. Geochimica et Cosmochimica Acta, 27, 1209–1264.

Morgan, J.W., and Wandless, G.A. (1980) Rare earth element distribution in some hydrothermal minerals: Evidence for crystallographic control. Geochimica et Cosmochimica Acta, 44, 973–980.

Munoz, J.L., and Eugster, H.P. (1969) Experimental control of fluorine reactions in hydrothermal systems. American Mineralogist, 54, 943–959.

Munoz, J.L., and Ludington, S. (1974) Fluoride-hydroxyl exchange in biotite. American Journal of Science, 274, 396–413.

Oakes, C.S. (1985) Strong salinity gradients in the northeastern part of the Salton Sea geothermal field, CA: A fluid inclusion and brine chemistry study. Geological Society of America Abstracts with Programs, 17, 679.

Petersen, E.U., Essene, E.J., Peacor, D.R., and Valley, J.W. (1982) Fluorine end-member micas and amphiboles. American Mineralogist, 67, 538–544.

Plimer, I.R. (1984) The role of fluorine in submarine exhalative systems with special reference to Broken Hill, Australia. Mineralium Deposita, 19, 19–25.

Pomârleanu, V., and Sabliovschi, V. (1980) Contribution to the geochemistry of muscovite from Romania. 26th International Geological Congress, Paris, Abstracts, 1, 139.

Potter, R.W., II. (1977) Pressure corrections for fluid-inclusion homogenization temperatures based on the volumetric properties of the system NaCl-H_2O. U.S. Geological Survey Journal of Research, 5, 603–607.

Potter, R.W., II, and Brown, D.L. (1977) The volumetric properties of aqueous sodium chloride solutions from 0° to 500°C at pressures up to 2000 bars based on a regression of available data in the literature. U.S. Geological Survey Bulletin 1421-C, 36 p.

Purkayastha, B.C., and Chatterjee, A. (1966) On the uptake of strontium tracer by different forms of calcium sulphate. Journal of the Indian Chemical Society, 43, 687–693.

Queen, L.D., and Motyka, R.J. (1984) Changes in the Makushin geothermal system: Evidence from alteration mineralogy. Geological Society of America Abstracts with Programs, 16, 329.

Rashkova, D.M. (1981) Zonal phlogopite crystals from the Rossen copper-molybdenum deposit, district of Bourgas. Comptes Rendus de l'Académie Bulgare de Sciences, 34, 1529–1532.

Rimšaite, J. (1969) Evolution of zoned micas and associated silicates in the Oka carbonatite. Contributions to Mineralogy and Petrology, 23, 340–360.

Robert, J.L. (1976) Titanium solubility in synthetic phlogopite solid solutions. Chemical Geology, 17, 213–227.

Roedder, E. (1969) Varvelike banding of possible annual origin in celestite crystals from Clay Center, Ohio, and in other minerals. American Mineralogist, 54, 796–810.

——— (1970) Application of an improved crushing microscope stage to studies of the gases in fluid inclusions. Schweizerische Mineralogische und Petrographische Mitteilungen, 50, part 1, 41–58.

——— (1984) Fluid inclusions. Mineralogical Society of America Reviews in Mineralogy, 12, 644 p.

Rogers, N.W., Hawkesworth, C.J., Parker, R.J. and Marsh, J.S. (1985) The geochemistry of potassic lavas from Vulsini, central Italy and implications for mantle enrichment processes beneath the Roman region. Contributions to Mineralogy and Petrology, 90, 244–257.

Rye, R.O., Luhr, J.F., and Wasserman, M.D. (1984) Sulfur and oxygen isotopic systematics of the 1982 eruptions of El Chichón volcano, Chiapas, Mexico. Journal of Volcanology and Geothermal Research, 23, 109–123.

Samartsev, I.T., Ovsyannikov, I.I., and Inshina, V.M. (1980) Gypsum-anhydrite mineralization in some gold-ore deposits of the Central Urals. Izvestiya Akademii Nauk SSSR: Seriya geologicheskaya, no. 2, 70–74.

Sasada, M. (1985) CO_2-bearing fluid inclusions from geothermal fluids. Geothermal Resources Council, Transactions, 9, part 1, 351–356.

——— (1986) Anhydrite precipitation by low pressure boiling at DW-5 drill hole, Hohi geothermal area, Japan: Fluid inclusion evidence and geological significance. Geothermal Resources Council, Transactions, 10, 149–154.

Schulze, D.J., Smith, J.V., and Němec, D. (1985) Mica chemistry of lamprophyres from the Bohemian massif, Czechoslovakia. Neues Jahrbuch für Mineralogie Abhandlungen, 152, 321–334.

Shikazono, N., and Holland, H.D. (1983) The partitioning of strontium between anhydrite and aqueous solutions from 150° to 250°C. Economic Geology, Monograph 5, 320–328.

Shikazono, N., Holland, H.D., and Quirk, R.F. (1983) Anhydrite in Kuroko deposits: Mode of occurrence and depositional mechanisms. Economic Geology, Monograph 5, 329–344.

Shmakin, B.M. (1984) Causes and consequences of high contents of barium in sheet muscovite and phlogopite. In Non-metallic mineral ores. Proceedings of the 27th International Geological Congress, 15, 261–271.

Taguchi, S., and Hoyashi, M. (1983) Fluid inclusion study in some geothermal fields of Kyushu, Japan. Fourth International Symposium on Water-rock Interaction, Misasa, Japan, Extended Abstracts, 459–462.

Thompson, R.N. (1977) Primary basalts and magma genesis III. Alban Hills, Roman comagmatic province, central Italy. Contributions to Mineralogy and Petrology, 60, 91–108.

Tronnes, R.G., Edgar, A.D., and Arima, M. (1985) Titanium solubility in phlogopite: An experimental study on its potential as a P-T indicator for upper mantle–lower crustal rocks. Geological Association of Canada and Mineralogical Association of Canada Joint Annual Meeting, Program with Abstracts, 10, A63.

Valley, J.W., Petersen, E.U., Essene, E.J., and Bowman, J.R. (1982) Fluorphlogopite and fluortremolite in Adirondack marbles and calculated C-O-H-F fluid composition. American Mineralogist, 67, 545–557.

Volfinger, M., Robert, J.-L., Vielzeuf, D., and Nevia, A.M.R. (1985) Structural control of the chlorine content of OH-bearing silicates (mica and amphiboles). Geochimica et Cosmochimica Acta, 49, 37–48.

Washington, H.S. (1906) The Roman comagmatic region. Carnegie Institution Publication no. 57, 199 p.

Wentlandt, R.F. (1977) Barium-phlogopite from Haystack Butte, Highwood Mountains, Montana. Carnegie Institution of Washington Year Book 76, 534–539.

Yau, Y.-C., Anovitz, L.M., Essene, E.J., and Peacor, D.R. (1984) Phlogopite-chlorite reaction mechanisms and physical conditions during retrograde reactions in the Marble Formation, Franklin, New Jersey. Contributions to Mineralogy and Petrology, 88, 299–306.

Yoder, H.S., and Eugster, H.P. (1954) Phlogopite synthesis and stability range. Geochimica et Cosmochimica Acta, 6, 157–185.

Zhang, R. (1986) Sulfur isotopes and pyrite-anhydrite equilibria in a volcanic basin hydrothermal system of the middle to lower Yangtze River Valley. Economic Geology, 81, 32–45.

Manuscript received June 26, 1987
Manuscript accepted March 17, 1988

Appendix 1. Phlogopite crystallography

A handpicked euhedral phlogopite crystal from 2210 m containing primary fluid inclusions but relatively free of trapped solids was examined by the single-crystal precession technique. The unit-cell data (Malcolm Ross, pers. comm., 1986) for the 2210-m crystal based on Buerger precession single-crystal photographs of the *h0l*, *h3hl*, *h3$\bar{h}$l*, 0k*l*, *hhl*, and *hh$\bar{l}$* nets are $a = 5.318$, $b = 9.228$, $c = 10.070$ Å, $\beta = 100.2°$, space group = $C2/m$.

The crystal examined is twinned by spiral $\pm 60°$ rotations of the individual layers (twinning about [110] and [1$\bar{1}$0]). The space group, $C2/m$, corresponds to the *1M* form. The *1M* form occurs throughout the entire range of geologic, physical, and chemical conditions (Yoder and Eugster, 1954).